

Final Report

Development of a Calibration System for the Laboratory Proctor (Soil Density) Mechanical Compaction Hammer

**FDOT Contract No. BD-545 #77
UF Contract No. 66761**

FDOT Project Manager: John Shoucair, P.E.
UF Principal Investigators: David Bloomquist P.E.
Michael McVay
Graduate Students: Keith Beriswill
Scott Wasman



January 30, 2008

DISCLAIMER

“The opinions, findings, and conclusions expressed in this publication are those of the authors and not necessarily those of the Florida Department of Transportation or the U.S. Department of Transportation”.

Prepared in cooperation with the State of Florida Department of Transportation and the U.S. Department of Transportation.

SI (Modern Metric) CONVERSION FACTORS (from FHWA)

Approximate conversions to SI units

SYMBOL	WHEN YOU KNOW	MULTIPLY BY	TO FIND	SYMBOL
LENGTH				
in	inches	25.4	millimeters	Mm
ft	feet	0.305	meters	M
yd	yards	0.914	meters	M
mi	miles	1.61	kilometers	Km
SYMBOL	WHEN YOU KNOW	MULTIPLY BY	TO FIND	SYMBOL
AREA				
in ²	Square inches	645.2	square millimeters	mm ²
ft ²	Square feet	0.093	square meters	m ²
yd ²	square yard	0.836	square meters	m ²
ac	acres	0.405	hectares	Ha
mi ²	square miles	2.59	square kilometers	km ²
SYMBOL	WHEN YOU KNOW	MULTIPLY BY	TO FIND	SYMBOL
VOLUME				
fl oz	fluid ounces	29.57	milliliters	ml
gal	gallons	3.785	liters	L
ft ³	cubic feet	0.028	cubic meters	m ³
yd ³	cubic yards	0.765	cubic meters	m ³
NOTE: volumes greater than 1000 L shall be shown in m ³				
SYMBOL	WHEN YOU KNOW	MULTIPLY BY	TO FIND	SYMBOL
MASS				
oz	ounces	28.35	grams	G
lb	pounds	0.454	kilograms	Kg
T	short tons (2000 lb)	0.907	megagrams (or "metric ton")	Mg (or "t")
SYMBOL	WHEN YOU KNOW	MULTIPLY BY	TO FIND	SYMBOL
TEMPERATURE (exact degrees)				
°F	Fahrenheit	5 (F-32)/9 or (F-32)/1.8	Celsius	°C
SYMBOL	WHEN YOU KNOW	MULTIPLY BY	TO FIND	SYMBOL
ILLUMINATION				
fc	foot-candles	10.76	lux	Lx
fl	foot-Lamberts	3.426	candela/m ²	cd/m ²
SYMBOL	WHEN YOU KNOW	MULTIPLY BY	TO FIND	SYMBOL
FORCE and PRESSURE or STRESS				
lbf	Pound force	4.45	newtons	N
lbf/in ²	Pound force per square inch	6.89	kilopascals	kPa

TECHNICAL REPORT DOCUMENTATION PAGE

1. Report No.	2. Government Accession No.	3. Recipient's Catalog No.	
4. Title and Subtitle Development of a Calibration System for the Laboratory Proctor (Soil Density) Mechanical Compaction Hammer		5. Report Date January 30, 2009	
		6. Performing Organization Code	
7. Author(s) David Bloomquist, Michael McVay, Keith Beriswill, Scott Wasman		8. Performing Organization Report No.	
9. Performing Organization Name and Address Department of Civil and Coastal Engineering 365 Weil Hall University of Florida Gainesville, FL 32611-6580		10. Work Unit No. (TRAIS)	
		11. Contract or Grant No. BD-545 #77	
12. Sponsoring Agency Name and Address Florida Department of Transportation 605 Suwannee Street, MS 30 Tallahassee, FL 32399		13. Type of Report and Period Covered Draft Final 3/30/07-12/31/08	
		14. Sponsoring Agency Code	
15. Supplementary Notes			
16. Abstract Existing techniques used to calibrate soil compaction equipment do not measure the overall imparted energy into the soil. Instead, various parameters (i.e., drop height, shoe weight, etc.) are measured independently and hence one is forced to assume that the theoretical energy is mobilized. Since the results of the Proctor density tests are critical to field compaction control, a calibration system is needed to ensure consistency in the equipment used by the Florida Department of Transportation (FDOT), consultant, and contractor testing labs. A new portable calibration device has been developed that measures rammer speed and base system forces during impact, and outputs the kinetic energy of the rammer. The calibrator was used to test 30 compactors in the state of Florida and it was discovered that the statistical variance of the data was acceptable. However, there was a trend indicating a lower than acceptable available energy for compaction. The results of this study will be used by labs to check and adjust their equipment so that results from disparate labs can be used with increased confidence. FDOT's Independent Assurance Inspection teams will also be able to provide a performance-based check.			
17. Key Word Calibrator, Kinetic energy, Proctor, Compaction, Density, Moisture content, Laboratory, Dynamic, Portable		18. Distribution Statement No restrictions.	
19. Security Classif. (of this report) Unclassified	20. Security Classif. (of this page) Unclassified	21. No. of Pages 94	22. Price

TABLE OF CONTENTS

	<u>page</u>
LIST OF TABLES	vii
LIST OF FIGURES	viii
EXECUTIVE SUMMARY	x
 CHAPTERS	
1 INTRODUCTION	1
1.1 Background.....	1
1.2 Problem Statement.....	3
1.3 Objective and Scope of Work.....	4
2 BACKGROUND	6
2.1 Mechanics of Compaction	6
2.2 Delivered Energy and Soil Compaction	6
2.3 Previous Research on Energy Measurement.....	8
2.4 Previous Research on the Variability of Soil Compaction Process	8
2.5 Base Compliance	9
3 DEVELOPMENT OF THE PORTABLE CALIBRATOR.....	12
3.1 Operation of the Compaction Machine.....	12
3.2 Fundamentals of the Calibrator.....	12
3.3 Conceptual Designs	14
3.3.1 Dynamic Impact Calibrator.....	14
3.3.2 Displacement Based Calibrator.....	16
3.3.3 Acceleration Based Calibrator	20
3.3.4 Development of the Photo Gate.....	22
3.3.5 The Infrared Photo Gate.....	23
3.3.6 Development of a Photo Electric Gate.....	26
3.4 Development of the Load Cell System	28
4 VALIDATION OF THE PORTABLE CALIBRATOR.....	29
4.1 Validation of the Photo Electric Gate	29
4.2 Accuracy of the Instrument.....	33
4.3 Validation of the Testing Procedure	34
4.3.1 Photo Electrics	34
4.3.2 Compliance Instrumentation.....	35
5 LABORATORY TESTING AND DATA ANALYSIS.....	37
5.1 PDEC Setup Description.....	37
5.2 Testing Program Overview	41

5.3	Testing Results and Analysis	43
5.3.1	Kinetic Energy Assessment	43
5.3.2	Manual Compaction Rammer	49
5.3.3	Base Compliance	50
5.3.4	Force Compressive Energy Theory	52
5.3.5	Compressive Energy Results	53
6	CONCLUSIONS AND RECOMMENDATIONS	56
6.1	Calibration Conclusions and Recommendations	56
6.2	Data Analysis Conclusions and Recommendations	57
6.3	Conclusions	57
	LIST OF REFERENCES	58
APPENDIX		
A	OPERATION OF INSTRUMENTATION	A-1
	The Photo Electric Gate	A-1
	Saving and Importing Data into Excel	A-2
	Kinetic Energy Processing	A-3
	Compliance Measurement Setup and Testing	A-3
	Compliance Energy Processing	A-4
B	LABORATORY DATA	B-1
C	RAMMER HEAD TESTS	C-1
D	SOIL DENSITY RESULTS FROM RAMMER HEAD TESTS	D-1

LIST OF TABLES

<u>Table</u>		<u>page</u>
3-1	Summary of Displacement Laser Energy Measurements	18
3-2	Measured Travel Times from Sensors and Corresponding Energy Calculations	26
4-1	Summary Statistics for Validation Study Hammer Rotations	32
B-1	T-180 Rammer Rotation Summary Statistics Per Machine	B-2
B-2	T-180B Base Compliance Summary Per Machine	B-3
C-1	Summary Statistics of Density Results	C-6
D-1	Coastal Soil Densities for Single Sector Rammer	D-2
D-2	Spring Cemetery Soil Densities for Single Sector Rammer	D-3
D-3	Branch Soil Densities for Single Sector Rammer	D-4
D-4	Iron Bridge Soil Densities for Single Sector Rammer	D-5
D-5	Summary of Densities from Double Sector Compaction Tests	D-6

LIST OF FIGURES

<u>Figure</u>		<u>page</u>
1-1	Effect of compaction energy on compaction of sandy clay	2
2-1	Effect of moisture content on dry density	7
2-2	Compaction foundation block with wood cushion in place	10
2-3	Effect of wood cushion on soil A-1-b Proctor curve.....	10
2-4	Effect of wood cushion on soil A-3 Proctor curve.....	11
2-5	Effect of wood cushion on soil A-2-4 Proctor curve.....	11
3-1	Typical mechanical soil compactor	13
3-2	Manual rammer frame	15
3-3	Compaction laboratory mechanical compactor displacement laser	17
3-4	Laser recorded displacement versus time plot	18
3-5	Detail of guide rods and guide disk.....	19
3-6	Typical acceleration record	21
3-7	Standard test setup for infrared photo gate.....	24
3-8	Voltage measured from infrared photo detector pairs 1, 2 and 3	25
3-9	Base mounted setup for fiber optic photo gate.....	27
4-1	Linear acceleration of rammer during T-180 fall.....	30
4-2	Sensor alignment on compaction machine.....	31
4-3	Typical acceleration and time duration plot for base compliance measurement	36
4-4	Typical force and time duration plot for base compliance measurement.....	36
5-1	Photo electric gate – Front view.....	37
5-2	Photo electric gate – Rear view.....	38
5-3	Illustration of rammer road at switching point of sensor 2	38

5-4	Data acquisition system setup and sensors.....	39
5-5	Base system configuration with mold assembly	40
5-6	Instrumented mold assembly.....	40
5-7	FDOT district map.....	41
5-8	Compactor foundation with steel cushion	42
5-9	Compactor foundation with plywood cushion	43
5-10	Frequency distribution of mean energy data	44
5-11	Bootstrap frequency distribution of mean energy	46
5-12	Frequency distribution of all energy data.....	47
5-13	Scatter plot of energy standard deviation versus mean velocity	48
5-14	Scatter plot of energy standard deviation versus mean energy	48
5-15	Frame for maintaining vertical alignment of rammer	50
5-16	Scatter plot of average maximum force	51
5-17	Scatter plot of average maximum acceleration	52
C-1	Modified Proctor sample prior to compaction	C-1
C-2	Modified Proctor sample after compaction	C-2
C-3	Sector rammer heads: (a) single; and (b) double.....	C-3
C-4	Pressure scan image results of single sector head	C-4
C-5	Average compaction results of branch, coastal, Florida rock soils	C-5

EXECUTIVE SUMMARY

This project involved research and development of a portable dynamic energy calibrator for mechanical Proctor compaction machines. Existing calibration methods do not measure the overall energy provided by a compactor system, and therefore, cannot accurately assess the summative energy imparted during the compaction process.

The research explored different options for measuring the rammer energy at impact. Considering the requirements of a device's functionality and complexities inherent in attachment to the compactor, the final design utilizes optical photo gates to monitor the drop speed of the rammer just prior to impact. In addition, a force transducer is attached to measure the impact force transmitted through the base of the machine. From these measurements, plus the rammer mass, the kinetic energy available for compaction and the energy absorbed by the base (via the impedance of the load cell) are known in real time for comparison to American Society for Testing and Materials (ASTM) standards.

The various system components were found to influence the compaction results, i.e., maximum dry density and optimum moisture content. That is to say, they affected the available compactive energy by issues associated with operator differences, possible variations in drop heights and the effects of base stiffness. The coefficient of variance for each of these variables should sum to the coefficient of variation of soil densities for a sample population tested on the same machine. This research thus focused on the design and construction of a calibrator that quantifies the energy and uncertainty associated with soil compaction.

The developed portable dynamic energy calibrator (PDEC) was tested on thirty compaction machines in three Florida Department of Transportation (FDOT) districts. Results indicated that energy variance within each machine was largely due to maintenance issues. More importantly, the research showed that the variance in the developed kinetic energy among the

sample population was small. However, there was a large variance associated with the compactor base compliance. The small variance in kinetic energy indicates that all machines tested operate nearly the same in terms of mass and drop height. The large variance in the base system energy is due to the various types of compactor support construction. While most compactors had some form of stiff cushion (aluminum, steel, concrete), the foundation varied between concrete cast in place (solid concrete mass) to mortared concrete blocks (void spaces). More significantly, the mean value of the kinetic energies was approximately 10% less (i.e., 15 ft-lb) than American Association of State Highway Transportation Officials (AASHTO) and ASTM standards.

In summary, the PDEC was developed to accurately determine the energy delivered in mechanical Proctor compactors. In addition, the requirements of portability and providing real time results were met. FDOT can now use this device to monitor compaction users and verify that the theoretical energy delivered to the soil sample is accurate. If there is deviation from the correct value, the data provided by the system can identify the source(s) of error.

CHAPTER 1 INTRODUCTION

1.1 Background

The Florida Department of Transportation (FDOT) and many other entities rely on the compaction of soil for infrastructure construction projects. This requires that a sample of onsite soils be compacted in a laboratory, in order to establish the requirements for field compaction. Explicitly, the characteristics of interest are the maximum dry unit weight and the optimum moisture content of the particular soil. Whether the test is being performed by the FDOT or by a private consulting laboratory, the testing procedure remains unchanged.

The Proctor compaction test consists of two primary types of tests; the Standard American Association of State Highway Transportation Officials (AASHTO) T-99 and the Modified AASHTO T-180 test. For each test, a rammer of a specified size, shape and mass is lifted to a specified height and allowed to fall until reaching a soil sample. The material is contained in a mold of specified size for a set number of impacts per soil lift. As a result of the rammer impact, compaction or densification of the soil occurs and should be directly related to the amount of energy that is produced. For a given compaction test, the amount of total energy that is delivered to a volume of soil is:

$$E = \frac{\left(\begin{array}{c} \text{number of} \\ \text{blows per} \\ \text{layer} \end{array} \right) \times \left(\begin{array}{c} \text{number} \\ \text{of} \\ \text{layers} \end{array} \right) \times \left(\begin{array}{c} \text{weight} \\ \text{of} \\ \text{hammer} \end{array} \right) \times \left(\begin{array}{c} \text{height of} \\ \text{drop of} \\ \text{hammer} \end{array} \right)}{\text{volume of mold}} \quad (1-1)$$

With an increase in applied energy, an increase in dry density will likely occur if the soil moisture content is maintained (Proctor 1933). Additionally, the optimum moisture content of the soil will vary for different amounts of energy imparted to the soil (Dubose 1952). This dependency of maximum dry unit weight and moisture content on energy is illustrated in Figure

1-1. Due to the effect of compaction energy on the resulting densities, it is critical that the energy and testing procedure be consistent. In this illustration, mass and drop height remained constant while the number of blows per layer increase and is representative of adding energy imparted to the soil.

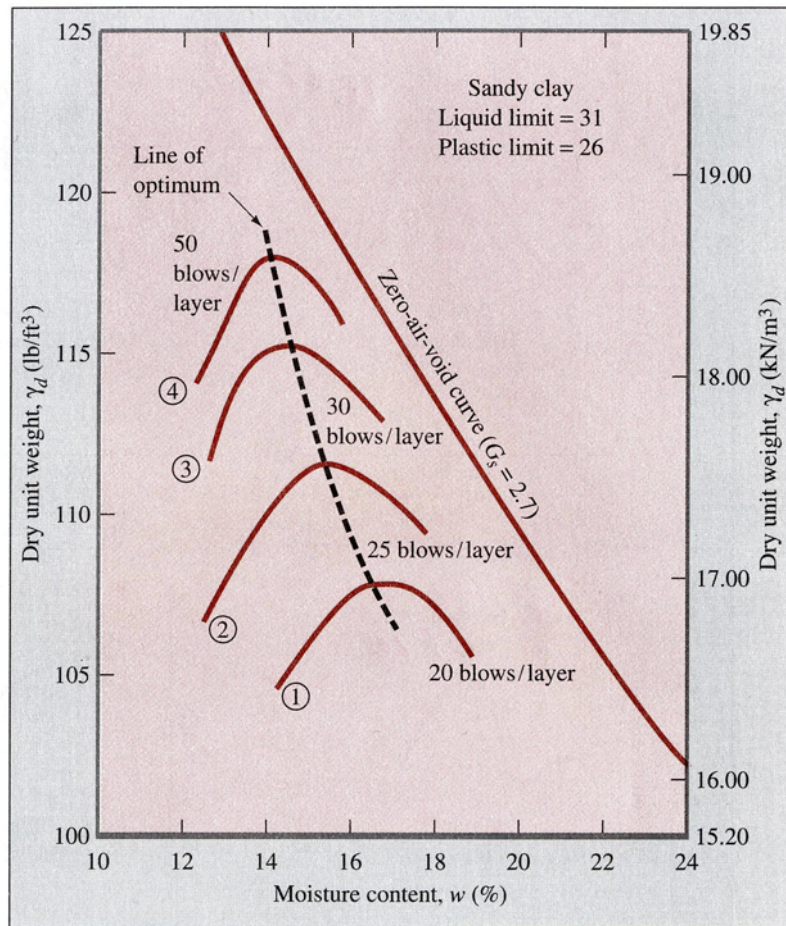


Figure 1-1. Effect of compaction energy on compaction of sandy clay (Das 2002).

In an effort to verify that mechanical compaction machines are delivering the prescribed energy, a calibration procedure is periodically performed. One calibration method, specified by AASHTO, is based on the deformation a lead cylinder upon rammer impact (ASTM D 2168 B). However, the method used by the FDOT utilizes the compaction of a calibration clay (CL)

material as prescribed by ASTM D 2168 A. For this method, the CL material is compacted using a manual Proctor compactor and the results compared to a specific machine to be calibrated (AASHTO T-99 or T180). Utilizing the manual testing procedure, the maximum dry unit weight and optimum moisture content of the soil are determined. It is then performed using the mechanical method (AASHTO T-99 or T-180) and the maximum dry unit weight compared. Attention is focused on the percent difference between the two maximum dry unit weights. When the absolute percent difference between the maximum dry unit weights for the two testing procedures is less than 2%, the mechanical calibrator is considered to be calibrated.

1.2 Problem Statement

In previous work performed by the FDOT, large quantities of soil were obtained, divided, and sent to state-approved private testing laboratories that use compaction machines calibrated via AASHTO D 2168 A. These samples were then tested in accordance with AASHTO specifications for the AASHTO T-99 Standard and AASHTO T-180 Modified testing procedures. The results from this testing regime displayed differences in the maximum dry densities and optimum moisture content reported from lab to lab. There appear to be two primary possibilities for these differences. Since the same soil was used for all testing, the possibility of soil properties skewing the results was assumed to be negligible. Thus, it was hypothesized there is some difference in the compactive energies across labs, or the operator had an effect on the results.

While the energy applied to the soil specimen is known to have a pronounced effect on density, it is not the only factor that needs to be considered. Base support can play a critical effect on both density and optimum moisture content (Chapman and Ray 1954). Knowing that

different base conditions do exist between laboratories, this research was launched to investigate both energy delivery and energy dissipation on resulting densities.

1.3 Objective and Scope of Work

As a result of the discrepancies in the maximum dry unit weight and optimum moisture content, the primary goal of this research was to take an energy based approach to the calibration of mechanical soil compactors. This involved being able to measure the energy available for compaction and the energy transferred to the base (base compliance) of the compaction machine. A portable calibration device was developed which measures both the rammer impact velocity and base system energy. It was then tested throughout FDOT district compaction laboratories.

The construction and validation of the device was performed at the Department of Civil and Coastal Engineering Laboratory at the University of Florida (UF) in Gainesville. Tests in several districts were performed on a population of thirty machines - mostly as AASHTO D T180 Modified compactors. The results were compiled and analyzed to establish a confident variance in energy available for compaction and base system energy. As components of the compaction process, these two quantifiable values comprise two-thirds of it, with the variance of the operator involving such things as moisture control, layer thickness, particle distribution, pre-tamping, and moisture determination. This issue was only identified as a contributor in soil density variance, as the time required for a testing was not available.

The scope of work found that the variance in compaction energy was half the variance in the base system energy. Although the compaction variance was small indicating similarity among machines in the test population, the mean energy was less than that prescribed by AASHTO T180 and ASTM D 1557 Standards. The difference is attributed to machine performance due to drop height and impact velocity, and not on the mass of the rammer.

Variance in base system energy is attributed to the many different base foundations discovered in the population. Typically, foundations consisted of some form of concrete, either cast or constructed with concrete blocks, and cemented in place.

CHAPTER 2 BACKGROUND

2.1 Mechanics of Compaction

Soil compaction is performed for the purpose of increasing the strength of the soil through densification (Proctor 1933). The process by which this increased density is reached is through the removal of air voids between soil particles (Das 2002). With the removal of the air voids, it is possible to increase the mass of soil in a finite volume. In order to most efficiently remove air, water is added allowing the soil particles to slide past one another as mechanical energy is applied. When the same amount of energy is applied and the amount of water is increased, eventually a maximum mass of soil will result. From this point on, the addition of water will serve to displace soil particles resulting in decreased density (Figure 2-1).

2.2 Delivered Energy and Soil Compaction

The energy that an object possesses in free fall is the sum of its potential and kinetic energy (Equation 2-1). In this situation it can be assumed that the instant the rammer is at its apogee, its velocity is zero. Thus, the rammer possesses only potential energy and its kinetic energy is zero (Equation 2-2). This case is opposite at the instant that the hammer has fallen and just prior to impact. Here, the object has no potential energy but possesses only kinetic energy (Equation 2-3) (Halliday 2000).

$$\text{Total energy} = (\frac{1}{2} \text{ mass} \times \text{velocity}^2) + (\text{mass} \times \text{gravity} \times \text{height}) \quad (2-1)$$

$$\text{Energy at drop height} = (\text{mass} \times \text{gravity} \times \text{height}) \quad (2-2)$$

$$\text{Energy at impact} = (\frac{1}{2} \text{ mass} \times \text{velocity}^2) \quad (2-3)$$

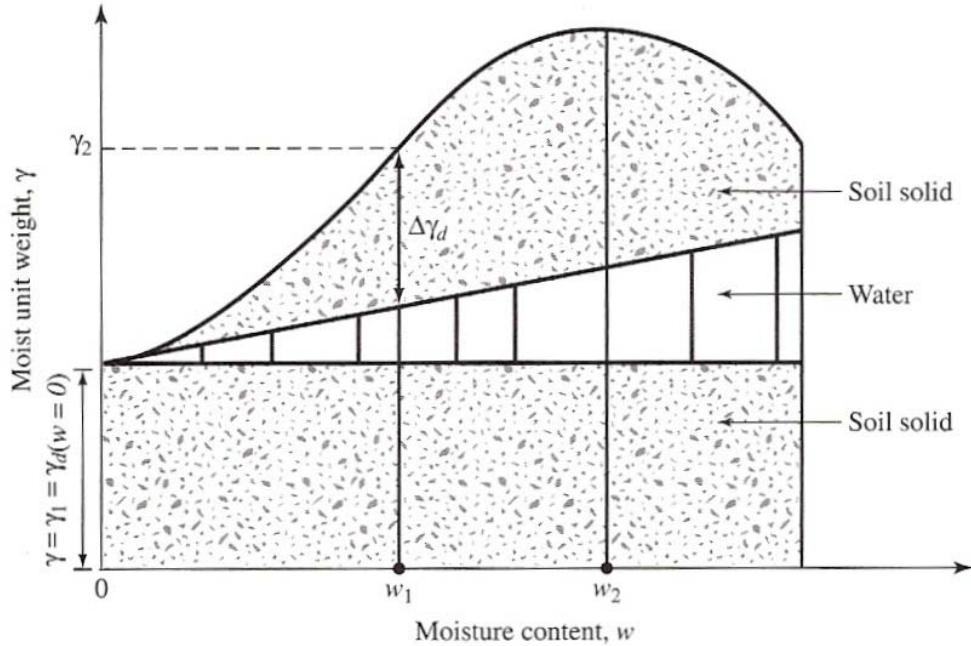


Figure 2-1. Effect of moisture content on dry density (Das 2002).

Based on conservation of energy, if the loss due to friction is negligible, then the energy at the drop height is equivalent to the energy at the instant of impact. The drop height and mass are each specified in AASHTO, and once verified to be within tolerance, the velocities for the T-99 and T-180 tests can be calculated through simple algebra.

AASHTO T-99 calls for a 5.5-lb rammer to be dropped 12 inches, thus producing 5.5 ft-lb of energy each drop. The T-180 method calls for a 10-lb rammer to be dropped 18 inches, resulting in a theoretical energy of 15 ft-lb being delivered (neglecting friction). AASHTO does however make allowance for differences in the drop height mass of the rammer for both testing procedures. This is ± 0.06 inches and ± 0.02 lb, respectively. Assuming the reduction in energy is negligibly affected by friction, for the Standard Proctor compaction test this results in a range of acceptable energy of 5.45 to 5.55 ft-lb. For the Modified Proctor compaction tests, the range is 14.92 to 15.08 ft-lb.

2.3 Previous Research on Energy Measurement

The Transportation Research Board (TRB) has published research that took an energy based approach to monitoring the compaction process. It also used the technique for soil compactor calibration (Sebesta and Liu 2007). Sebesta and Liu's research focused on a permanently mounted displacement sensor that utilized a magneto-restrictive rod and sensing ring concentrically mounted above the rammer rod.

While this method may be used in a particular lab to measure the impact velocity of a rammer, it does not appear that it lends itself for use on multiple machines in other labs, nor could it be used to establish the energy delivered from a manual compaction hammer. The study proved useful in measuring impact velocity but proved to be ineffective as a portable energy calibrator due to the permanent mounting requirements of the displacement sensor.

Most critically, they found that successive impacts of a mechanical compaction rammer do not provide equal energy. This means that multiple successive impacts needed to be monitored.

2.4 Previous Research on the Variability of the Soil Compaction Process

Reproducibility of soil compaction has been previously investigated using a 2.5-kg and 4.5-kg (5.51-lb and 9.92-lb) rammer, comparable to the T-99 and T-180 testing procedures by British standards for both manual and mechanical compactors. According to The Roadway Research Laboratory, "No significant differences could be observed between the results achieved by hand compaction and those achieved by machine compaction" (Sherwood 1970). In terms of the observations made in this research, it was also noted that no faulty hand held rammers were observed in any laboratories and that the masses and drop heights of all handheld rammers were consistent. Thus, they concluded that differences in testing using the handheld rammer could only be documented by observing the actual test.

Of primary interest in their study was the effect a single operator had on soil density and optimum moisture content results, as well as the effect of different laboratories. Their results showed that an operator using the same machine to run multiple tests showed little variance, with a maximum dry density COV of 0.13 and 0.84 for optimum moisture content, whereas eight operators on a single machine had a maximum dry density COV of 2.8 and 7.8 for optimum moisture content for the same soil. The Road Research Laboratory then looked at results for 36 laboratories and found a COV of 2.1 for maximum dry density and 9.7 for moisture content. These results illustrate that the testing procedures of a single operator tend to be far more consistent than between individuals or different laboratories. The research did not seek to identify the source of the differences between the laboratory testing results in terms of the mechanical compaction equipment (Sherwood 1970).

2.5 Base Compliance

In UF research, an effort to determine the effect of a worse-case scenario regarding the base stiffness of a mechanical compactor was investigated. Two 0.75-inch thick plywood sheets were bolted to the top of a concrete compaction foundation block in the Soils Compaction Lab (Figure 2-2).

Six manual T-99A tests were then performed, two each on A-3, A-1-b and A-2-4 soils; one with and one without the plywood cushion. As expected, the boundary condition had a profound effect on the shape of the compaction curve as well the maximum dry density (Figures 2-3, 2-4, 2-5). The resulting density varied between 0.7% and 3.4% lower with the wood base compared to the T-99A standard procedure. For the A-3 soil, the optimum moisture content varied by more than 1%.

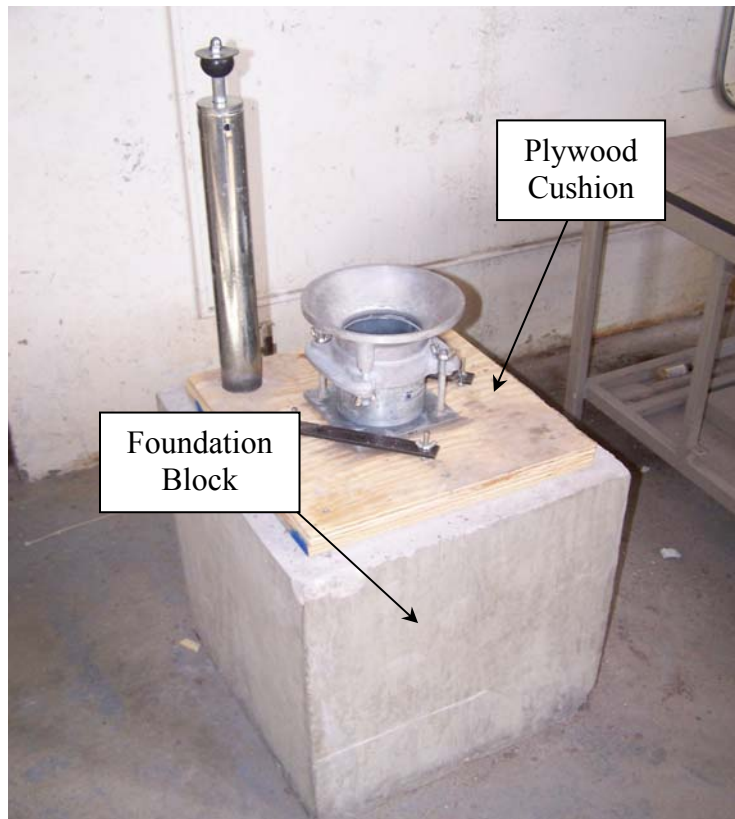


Figure 2-2. Compaction foundation block with wood cushion in place.

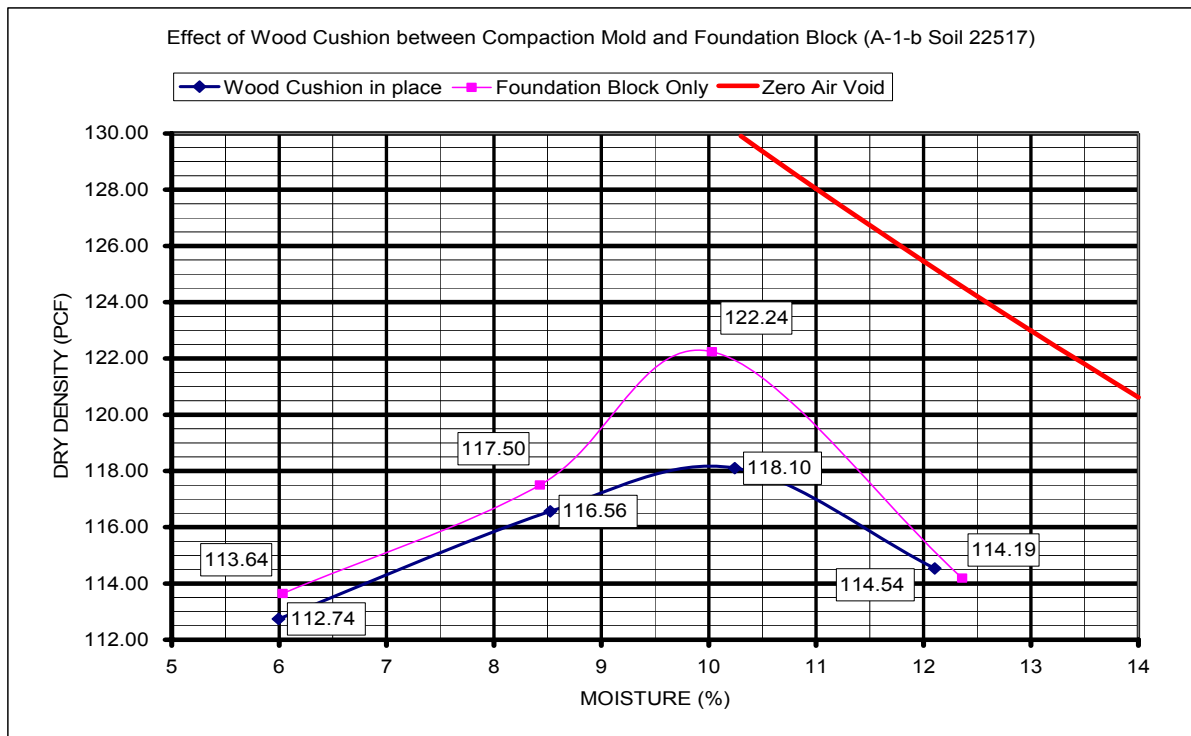


Figure 2-3. Effect of wood cushion on soil A-1-b Proctor curve.

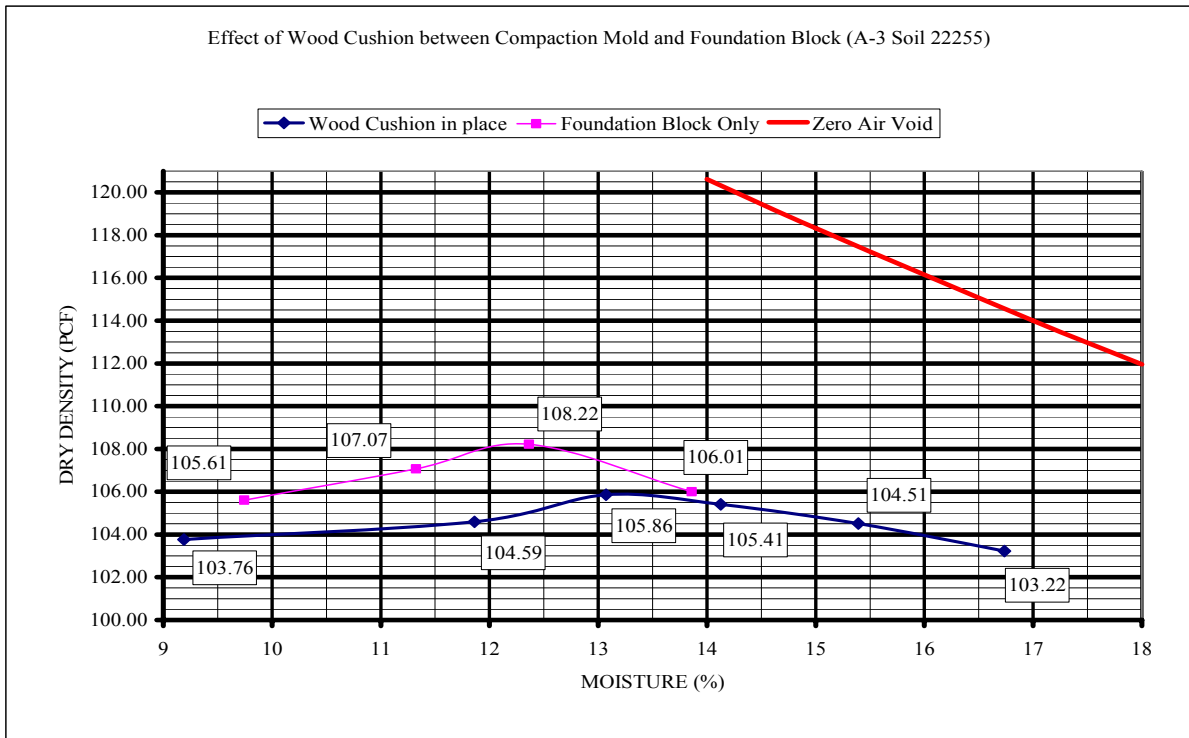


Figure 2-4. Effect of wood cushion on soil A-3 Proctor curve.

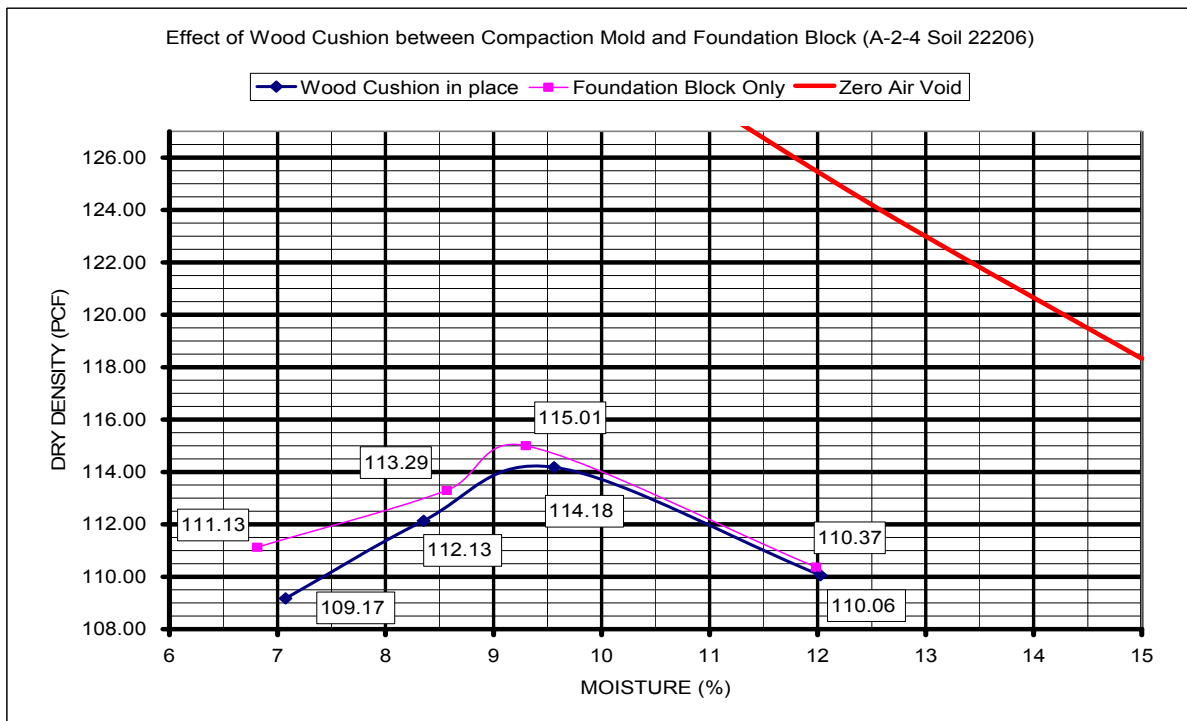


Figure 2-5. Effect of wood cushion on soil A-2-4 Proctor curve.

CHAPTER 3 DEVELOPMENT OF THE PORTABLE CALIBRATOR

3.1 Operation of the Compaction Machine

The typical compaction machine used consulting labs in Florida as well as the FDOT's State Materials Office (SMO) is the Rainhardt Model 662 or similar machine (Figure 3-1). This machine consists of an electric motor that drives a belt which rotates a flywheel and attached cable to lift a grabber vertically. The lift height is a calibrated, controlled distance specific to the test, either 12 ± 0.06 inches or 18 ± 0.06 inches. This grabber travels along the rammer rod and grabs the rod at its lowest point of travel, rotates the rod a fixed increment during the lift and releases it at the highest point of travel at which time the rammer rod falls vertically. While falling, the rammer rod passes through the jaws of the grabber and is guided by a disk on the rammer assembly along guide rods until impact. Figure 3-1 illustrates the main components of the mechanical compactor.

3.2 Fundamentals of the Calibrator

Development of an energy based calibrator required that the energy delivered to a soil sample be quantified. In order to perform this task, several general issues needed to be addressed. First, the rammer should be allowed to rotate freely during the compaction procedure. Secondly, the calibration device should function without altering the compactor, thereby voiding its calibration. This would then require a recalibration per AASHTO specifications prior to being used. Thirdly, no attachments to the rammer or guide rods are possible, since attaching any part of a calibrator to the rammer changes the rammer mass, and thus, the kinetic impact energy.



Figure 3-1. Typical mechanical soil compactor.

Observation at FDOT approved compaction laboratories indicated that in some, height above the compaction device was limited to less than 18 inches from the ceiling. This would have required cutting a hole in the ceiling to utilize Sebesta and Liu's device and thus was not pursued further.

3.3 Conceptual Designs

Several design strategies were formulated on ways the energy of a rammer compaction blow could be measured or calculated. In theory, quantification is a simple physics problem involving potential and kinetic energy and work theory. Using basic assumptions about the operation of the machine, these three aspects are related and it was determined that the energy might be measured through displacement, acceleration or the work done at impact via a dynamic load cell.

3.3.1 Dynamic Impact Calibrator

Initial instrumentation development focused on the principle that the kinetic energy of the rammer fall was equal to the work done. When the rammer impacts the soil, work is done as the soil deforms, the amount based on the soil's modulus. From the force measured during the deformation, one is able to employ the relationship between deformation and work (Equation 3-1). Assuming negligible losses occur, the work calculated would be the same as the energy that was delivered by the rammer.

$$W = \int_{y_1}^{y_2} F(y) dy \quad (3-1)$$

In this equation, W is the work done on the sample, F is the force applied to the specimen, and y is the deformation (compression) of the soil mass.

By inserting a dynamic force sensor at the location of the rammer impact point and measuring the displacement of the rammer during impact, Equation 3-1 could be calculated. In order to dampen the blow to protect the dynamic force sensor from excessive force and to provide measurable impact deformations, a relatively soft impact pad with known material properties was used.

A Micro-epsilon displacement laser with an operating frequency of 2,500 samples per second (2.5 kS/s) and precision of 0.001 of an inch was purchased for the project. In addition, a PCB 200C20 quartz piezoelectric analog dynamic force sensor with a range of 50,000 lb was acquired. The testing procedure consisted of conducting tests utilizing this instrumentation on a manual compaction hammer with different types of polyurethane and neoprene pads as the surface material. A two-inch diameter metal ring was installed on the compactor hammer to provide a target for the laser to reflect from. A frame was constructed to mount the laser displacement sensor. In addition, the frame contained two cross members with C-clamps in order to maintain vertical alignment of the hammer during a drop (Figure 3-2).



Figure 3-2. Manual rammer frame.

After several tests, this concept was abandoned since the hammer could not be moved around the mold as it would be during a compaction test run on mechanical compaction equipment. Based on this issue, allowing free rotation of the rammer became a high priority in the development of the calibration device.

3.3.2 Displacement Based Calibrator

Testing then focused on a displacement sensor that could measure the rammer's trajectory over its entire fall event. By utilizing an entire free fall set of data, the total displacement of the rammer for each impact could be determined (Equation 2-2, Section 2.2) and compared. However, more importantly, the impact velocity of the rammer also could be calculated and used to quantify the amount of kinetic energy that the rammer delivers with each impact (Equation 2-3, Section 2.2).

Using this knowledge and the goal of allowing free rotation of the rammer, testing began on the mechanical compactor. The mass of the rammer assembly was determined using a standard digital laboratory scale. A light (0.06-oz) metalized plastic disc target was affixed to the top of the rammer rod to serve as a target for the laser displacement sensor. The displacement transmitter/receiver was then mounted above the lift rod. Figure 3-3 illustrates the test setup. The full displacement record was then processed and analyzed to determine the total distance the rammer traveled over the course of the fall.



Figure 3-3. Compaction laboratory mechanical compactor displacement laser.

The displacements with respect to time were plotted and a second order trend line fitted through the data using Microsoft Excel. Refer to Figure 3-4 for a typical example of a plot. Using the trend line for each of these displacement records, the first derivative was then taken with respect to time. This results in a velocity profile equation for the fall and was then evaluated at the time of impact, providing a calculated impact velocity of the rammer for each impact. The impact velocity was then used to evaluate the kinetic energy. The results of a series of rammer drops, fall distance, impact velocity, potential energy, and kinetic energy for each drop are presented in Table 3-1.

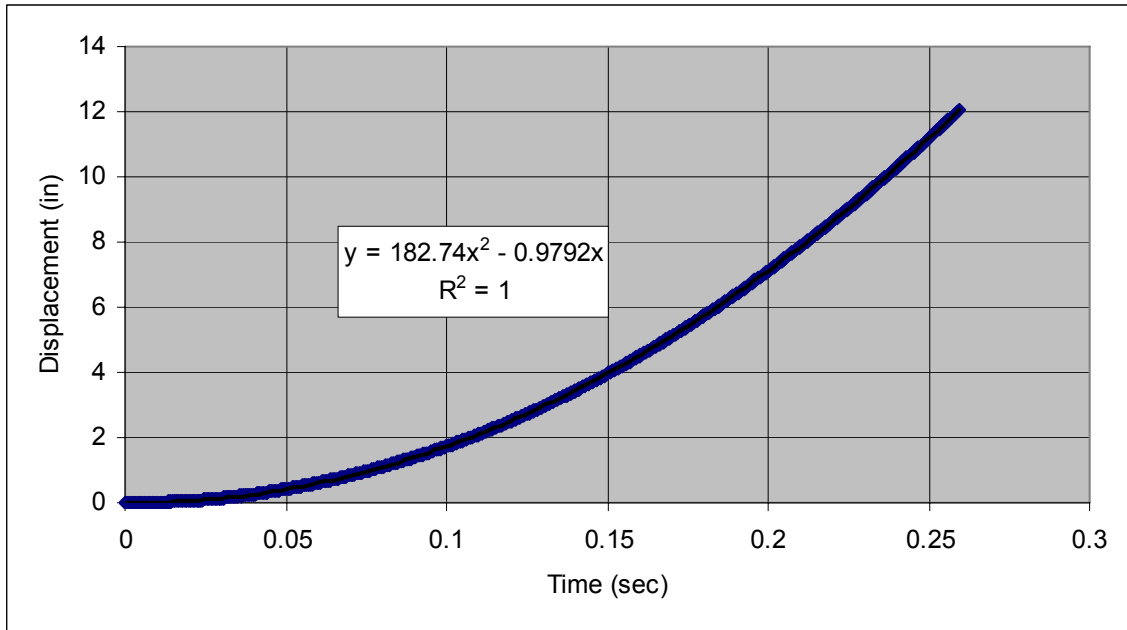


Figure 3-4. Laser recorded displacement versus time plot.

Table 3-1. Summary of Displacement Laser Energy Measurements (5.5-lb rammer)

Kinetic		Potential	
Velocity (ft/sec)	Energy (ft-lbs)	Displacement (in)	Energy (ft-lbs)
7.70	5.07	12.03	5.51
7.73	5.10	12.08	5.54
7.74	5.12	12.05	5.52
7.75	5.13	12.08	5.54
7.76	5.15	12.20	5.59
7.81	5.21	12.04	5.52
7.82	5.22	12.06	5.53
7.77	5.16	11.93	5.47
7.76	5.14	12.17	5.58
7.72	5.09	12.10	5.55

As expected, this table shows that in all cases, the kinetic energy is less than the potential energy. This is due to frictional losses from the rammer guide rods and disk contacting each other during free fall (Figure 3-5). It is important to note that the machine used at the UF compaction laboratory is not currently used for soil compaction but rather for prototype

development and validation. Hence, it has not been certified as calibrated. However for calculation purposes, the mean drop height measured for these 10 impact was 12.07 inches which is very close to the tolerance of 0.06 inches specified in AASHTO standards.

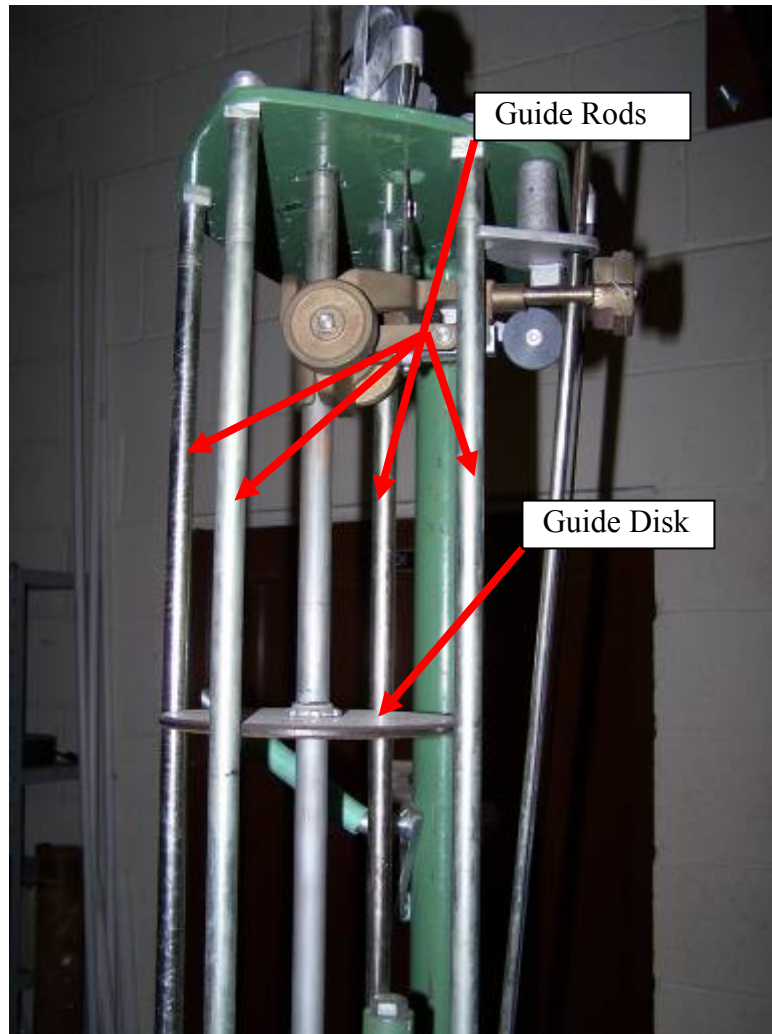


Figure 3-5. Detail of guide rods and guide disk.

These results verify that measuring the full rammer displacement during its fall may prove effective in accurately determining potential energy. Additionally, this study indicates there are significant differences in the actual versus theoretical kinetic energies, attributable to frictional losses. However, due to the mounting and clearance issues with the laser, its high cost and complexity of aligning the target with the laser, this concept was abandoned.

3.3.3 Acceleration Based Calibrator

The investigation then focused on using an accelerometer for determining the kinetic energy of an impact, since a miniature accelerometer could be easily mounted on the rammer without adding significant weight. The accelerometer provides information such as the rammer release point, the time of impact and the acceleration during the fall. A numerical integration of the acceleration data produces a velocity profile and more importantly, the impact velocity. A second integration could then be performed over the same time interval and the displacement of the rammer with time determined as well.

From the accelerometer information it was thought that one would be able to compare the theoretical potential energy to the actual potential energy as well as the kinetic energy just prior to impact. This kinetic energy would be a useful check against the energy calculated from the load cell.

However in practice when attempting this configuration, significant issues arose regarding the processing of the accelerometer data due to the vibration of the compactor during operation and the data having a high-frequency noise component in the signal. One of the impact records of a single lift and drop cycle is shown in Figure 3-6.

In the graph in Figure 3-6, it is possible to see the noise in the signal. The acceleration of the rammer was expected to be constant or nearly constant at approximately one g, the gravitational constant (32.2 ft/sec^2). As can be seen, Figure 3.6 shows that no clear acceleration record is evident.

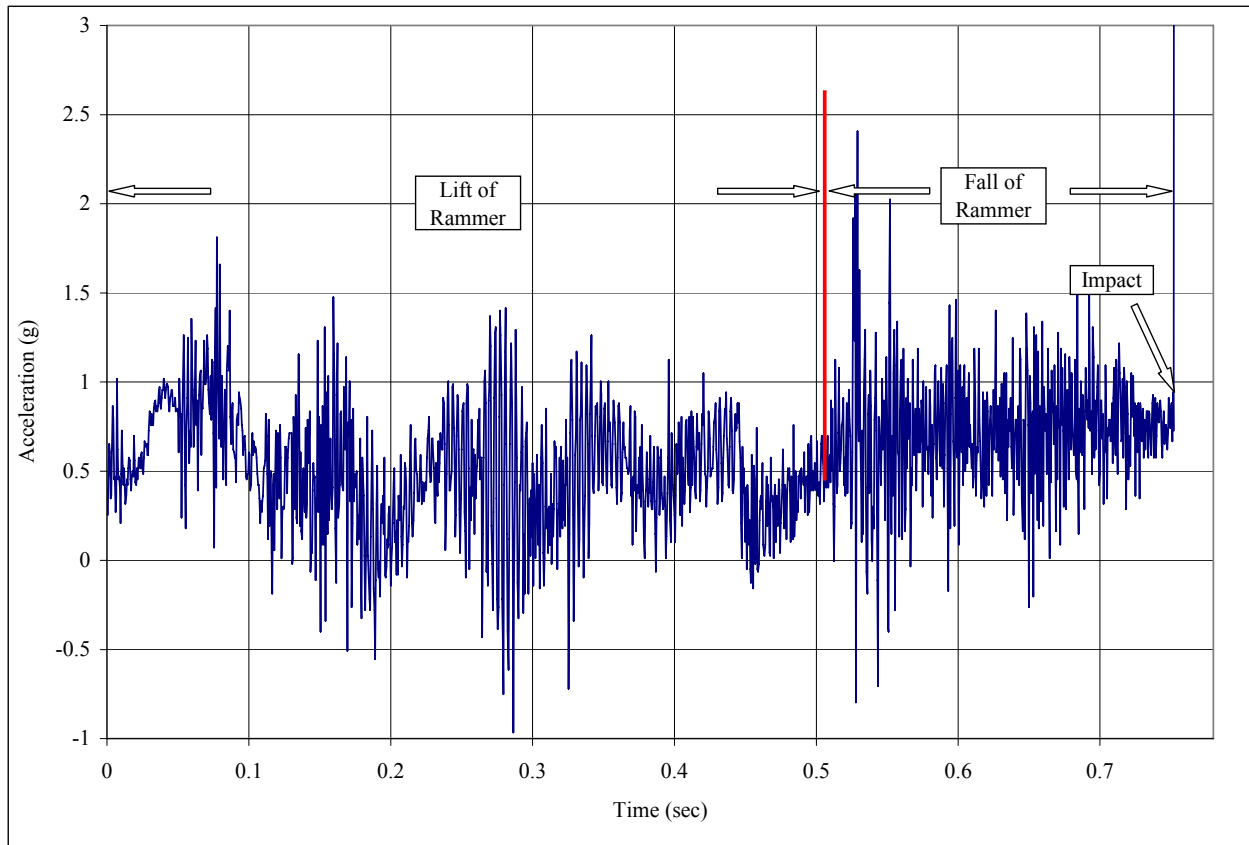


Figure 3-6. Typical acceleration record.

Advanced numerical signal processing utilizing a Fast Fourier Transform procedure was performed on the signal which indicated that during the lift portion of the cycle there was an underlying frequency of 10 Hz. This was attributed to vibration of the motor lifting the rammer. Following the point at which the rammer was released to begin its free fall, the noise frequency increased dramatically. This high frequency is likely caused by the rammer's guide disc contacting the guide rods during the fall. The high noise amplitudes occurred throughout the Fourier transform, making it nearly impossible to remove and obtain an accurate acceleration record. While it is possible that further advanced signal processing algorithms could have been employed, the time and effort required to obtain useful information was considered problematic. Since the goal of this project is to produce a relatively simple and repeatable device that does not

involve advanced data processing and lengthy computational effort, it was decided to abandon this approach and look at yet another alternative concept.

3.3.4 Development of the Photo Gate

Work began on a more direct way of measuring velocity, in order to compute the kinetic energy of the rammer assembly. A search for available velocity sensors was conducted and several transducers were identified. However due to the constraints of the testing environment (i.e., no added mass to the rammer, clearance issues, etc.), nothing was found that would work for this application.

Thus, obtaining an average velocity rather than an instantaneous velocity concept was pursued. Average velocity is readily computed by accurately measuring an elapsed time over a known distance. Equation 3-2 below provides results sufficiently close to the instantaneous velocity at impact as long as the distance over which the time measurements are taken are sufficiently small. This is illustrated mathematically by analyzing the limits of Equation 3-2 as Δd approaches zero, yielding the instantaneous velocity of the rammer. However, physically this is not possible as there is no way to measure change in time as the rammer passes a single point along its path.

$$\text{Velocity} = \frac{\Delta d}{\Delta t} = \frac{d_2 - d_1}{t_2 - t_1} \quad (3-2)$$

In order to apply this method, the rammer instrumentation needed to be set up to begin a trigger timer as the rammer passed a known point just prior to impact and a second sensor to measure the Δ time as the rammer passed a second point slightly closer to the point of impact. The second time measurement is then subtracted from the first and dividing by the distance between sensors, an average velocity is computed. By measuring the distance between the

sensors with a set of calipers accurate to 1/1000th of an inch, the distance between the sensors can be accurately measured. These measurements can then be inserted into Equation 3-2 and the velocity just prior to impact evaluated.

While investigating this concept, it was felt that the Hall effect or proximity sensors might be a viable choice. However, further investigation showed that it would be virtually impossible to mount such a assemblage of transmitters/receivers close to the point of impact without creating measurement errors. Thus, it was decided that another type of sensor would be investigated.

3.3.5 The Infrared Photo Gate

Based on the fact that the data acquisition system can readily read voltages, the idea emerged that a photo gate or optical switch might work. It is based on the principle that when a phototransistor detector senses an emitter diode's IR light, a voltage is produced. In addition, when the phototransistor detector does not sense the emission, the voltage remains zero. Three of these emitter/detector pairs were then planned to be mounted in sequence and used to obtain the change in time. The rationale for using three sensor pairs rather than two was based on the fact that if time measurements were known at three locations, then three separate velocity calculations were possible. These additional velocity measurements could then be used to determine if the velocity of the rammer was within an acceptable profile.

Several infrared emitter and detector pairs were purchased with the appropriate resistors in order to create the switch configurations. Switch operation was then monitored with a voltmeter for preliminary tests and found to perform properly. They were then mounted to a compaction mold base plate so that an emitter and its corresponding detector were on opposite sides of the plate (Figure 3-7).

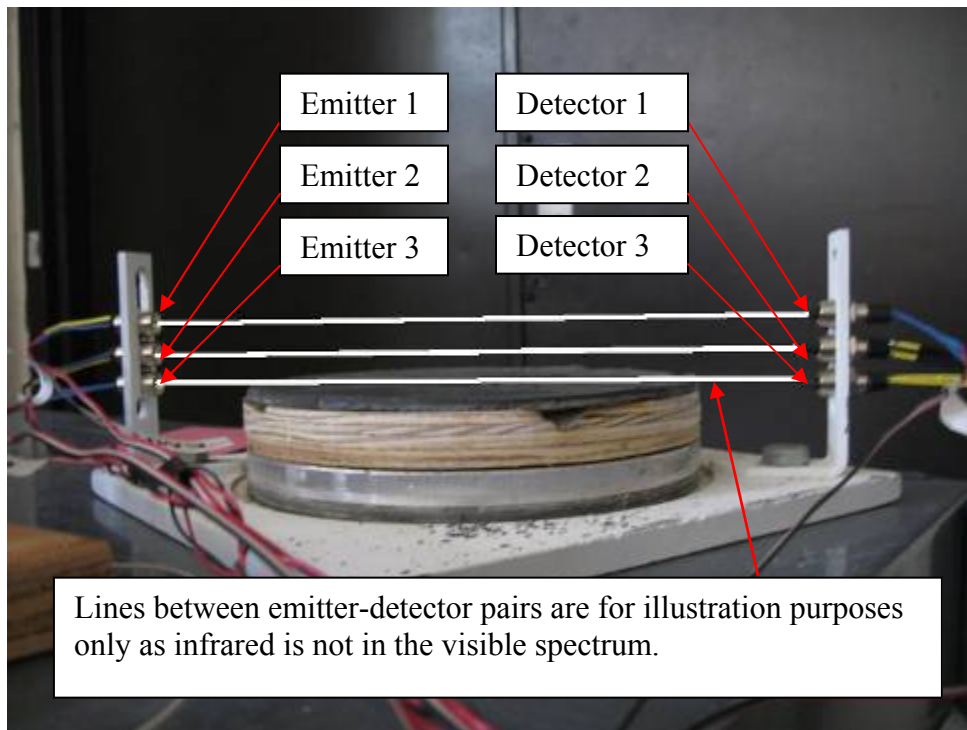


Figure 3-7. Standard test setup for infrared photo gate.

In order to prevent rammer bounce, an impact pad was added to dampen the blow. Various materials were tested, since it is important for it to not undergo any permanent deformation. This is because the distance from the surface to the last detector would then change slightly and alter the velocity calculations. Having a proper impact pad also allowed for the lower emitter and detector pair to be aligned such that the voltage drop will occur the instant the rammer comes into contact with the pad.

After numerous tests, several issues became evident. First, there were occasional voltage spikes prior to switch detection as well as random voltage irregularities. Effort was spent trying to eliminate interference from outside infrared sources, as these were suspected of causing the problem. The increase in voltage prior to impact was determined to come from the reflection of infrared light reflecting off the bottom of the rammer's face prior to the rammer actually

breaking the line of sight of the detector. These issues made it impossible to accurately determine the time of travel. An example of the data obtained from the infrared photo gate is presented in Figure 3-8.

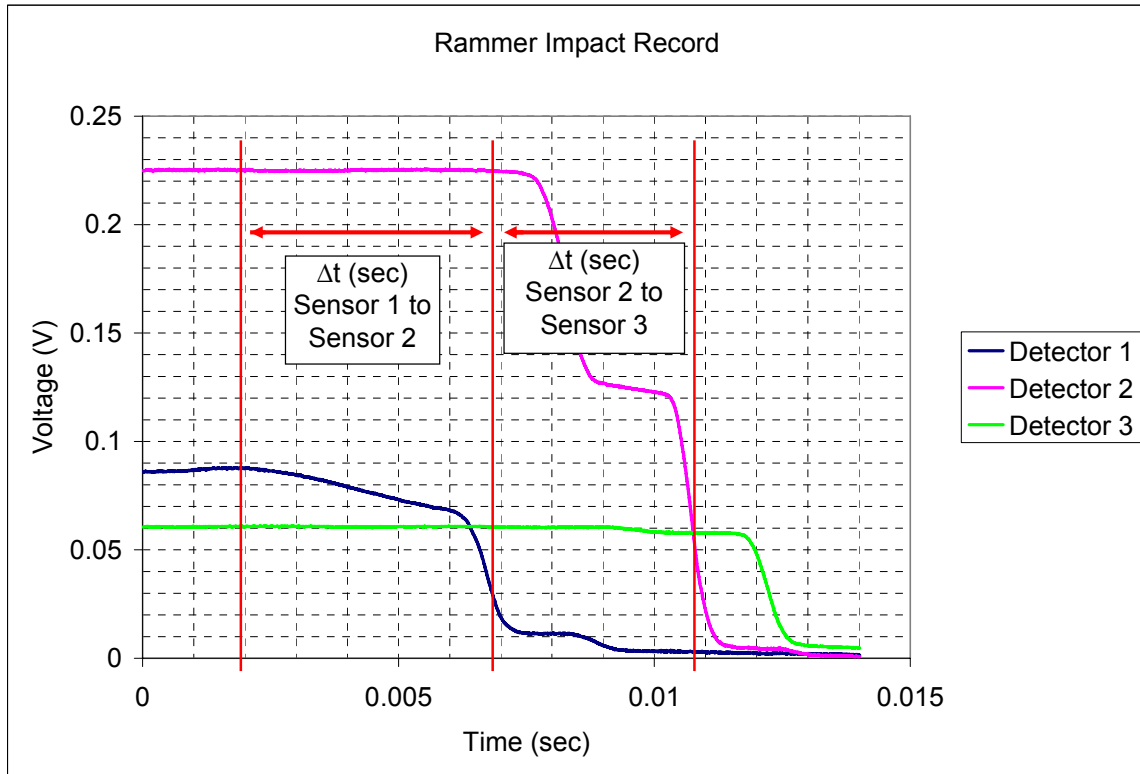


Figure 3-8. Voltage measured from infrared photo detector pairs 1, 2 and 3.

Several rotations of the hammer with ten impacts each were performed and velocities were calculated. These measured velocities were then compared to impact velocities obtained from differentiation of the laser's displacement record. The results are presented in Table 3-2.

Table 3-2 shows the importance in accurate time determination, since small differences in the measured time have a large adverse effect on the velocity calculations. It was determined that for accurate kinetic energy measurement, the infrared emitter detector sensors were not adequate unless significantly improved. Attempts were made to obtain better quality voltage records by

replacing the infrared emitted diodes with laser diodes, however, this also proved unsuccessful. Attention was then directed to an existing type of through-beam photo electric sensor which was available on the market.

Table 3-2. Measured Travel Times from Sensors and Corresponding Energy Calculations

Impact	Sensor 1 to Sensor 2 Δt (sec)	Sensor 2 to Sensor 3 Δt (sec)	V_1 Avg Velocity Sensor 1 to Sensor 2 (in/sec)	V_2 Avg Velocity Sensor 2 to Sensor 3 (in/sec)	Kinetic Energy	
					E_1 (from V_1) (ft-lb)	E_2 (from V_1) (ft-lb)
1	0.00486	0.00468	87.45	90.81	8.25	8.90
2	0.00314	0.00439	135.35	96.81	19.77	10.11
3	0.00856	0.00435	49.65	97.70	2.66	10.30
4	0.00761	0.00554	55.85	76.71	3.37	6.35
5	0.00680	0.00569	62.50	74.69	4.22	6.02
6	0.00412	0.00417	103.16	101.92	11.48	11.21
7	0.00462	0.00411	91.99	103.41	9.13	11.54
8	0.00656	0.00748	64.79	56.82	4.53	3.48
9	0.00670	0.00442	63.43	96.15	4.34	9.98
10	0.00254	0.00542	167.32	78.41	30.21	6.64

3.3.6 Development of a Photo Electric Gate

Traditionally, photo electric sensors have been utilized in manufacturing for product detection, but it was hypothesized and later proven that these sensors were able to effectively detect the presence of the rammer as it passed by a sensor in the same manner that the infrared sensors operated. The primary issue with these devices was their switching response times since all of the available models were digital (compared to analog).

After significant searching, Keyence Corporation had the precise instrument to resolve the issues encountered in the testing of the infrared photo gate. After reviewing the specifications, two Keyence FS-M1H fiber optic amplifiers were purchased. These sensors operate on the same

principle as the infrared photo gates in detecting the rammer's presence. However, they boast more advanced electronic features for velocity measurements.

The Keyence M1H fiber optic sensors operate digitally. They are essentially a switch in the traditional sense of the word, with the output from the sensor either a fixed portion of the excitation voltage or zero. This function allows for simple determination of when the rammer passes the line of sight of the detector. While detection remained an issue for the infrared sensor, it was not the only issue solved by using this instrument. The fiber optic sensors also offer a fixed sampling period of 20 microseconds which by calculation is more than sufficient for a spacing of 0.950 inches, the anticipated sensor spacing. These features alone are reason enough to utilize these sensors. In addition, they feature pair specific light modulation to prevent cross talking and false detections of the rammer which ensure accurate reporting of rammer detection times.

The sensor heads were mounted in the same configuration as the infrared sensors on the base plate of the compaction mold as a pair for testing (see Figure 3-9).

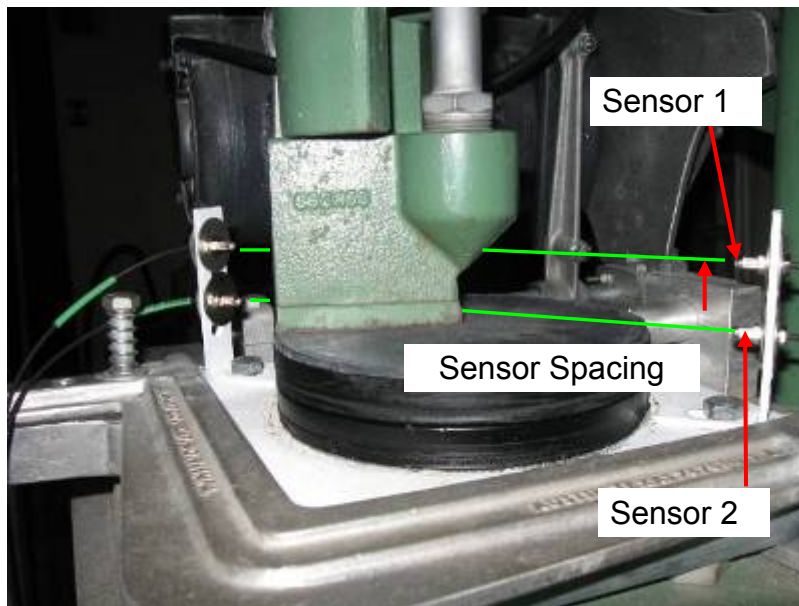


Figure 3-9. Base-mounted setup for fiber optic photo gate.

3.4 Development of the Load Cell System

During the development stage of measuring the impact kinetic energy, several compaction units were observed in various laboratories. It became apparent during these laboratory visits that while all of the machines were calibrated per AASHTO standards, there was one major difference that appeared fairly regularly. As per soil compaction standards, the compaction machine must be mounted on a rigid concrete base with a mass greater than 200 lb (AASHTO T-99 and T180 Note 7). All the machines observed did satisfy this requirement, however, some had a plywood cushion beneath their steel base plates while others used aluminum spacers. In fact, several had nothing supporting their bases.

As previously shown in Figures 2-1 through 2-3, an observable shift in the maximum dry density and the optimum moisture content occurs that is not consistent with AASHTO specifications. This is likely due to the varying amount of energy that is transferred into the soil during compaction. With the understanding of dampening and its energy effects, the possibility that the base stiffness itself may have a significant effect on soil compaction was surmised. In order to quantify what effect the base stiffness has on energy transfer, standard compaction mold base plates, 4 and 6 inch respectively, were instrumented with both a PCB 200C20 load cell and a PCB M352A60 accelerometer. A 0.25-inch thick piece of neoprene pad was then cut to fit the impact surface of the load cell to protect it during impact. These base plates were then fastened to the base of the machine and clamped in place. The compactor's rammer could then be set up at the standard drop height angled slightly from the impact pad to account for the rotation of the rammer. The machine could then be switched on for a single impact on the face of the load cell.

Due to the accuracy and ease of repeatability of this test, it could then be used to measure the base stiffness of a sample population of compaction machines. From this information, the energy losses due to variables in the mounting configuration of the machines could be quantified.

CHAPTER 4 VALIDATION OF THE PORTABLE CALIBRATOR

4.1 Validation of the Photo Electric Gate

In order to ensure accurate velocity measurements using the fiber optic photo gate, it was critical to compare the velocities measure with a known velocity. Thus, the laser displacement sensor was again mounted above the mechanical compaction machine and used to continuously measure the displacement of the rammer. The photo gates were mounted in the configuration pictured in Figure 3-9 as shown in Section 3.3.6. The mechanical compaction machine in the T-180 configuration, was then switched on and allowed to complete five full rotations of the impact rammer, in this case several of the impacts were missed by the photo gate when the rammer was near perpendicular to the sensor as discussed previously. For the 50 impacts, 29 were captured by the photo gate. However, this is not a problem, since the operator would simply wait until a sufficient number of data points are collected.

The displacement record from the laser was then parsed such that the data for the fall could be analyzed. This data was then processed in a very similar way to that presented in Figure 3-4. However, through a study of the laser displacement data, the acceleration was not constant. Using a central difference scheme on the displacement versus time records, accelerations for points along the time record were calculated directly. These results are presented in Figure 4-1.

The results clearly show the acceleration changes with respect to time linearly throughout the fall event of the rammer. This prevents use of a second-order equation for derivation of impact velocity of the rammer as a valid method. Rather, it dictates the use of a third-order polynomial equation for the description of the rammers fall with displacement in order to allow the linear change in acceleration with time.

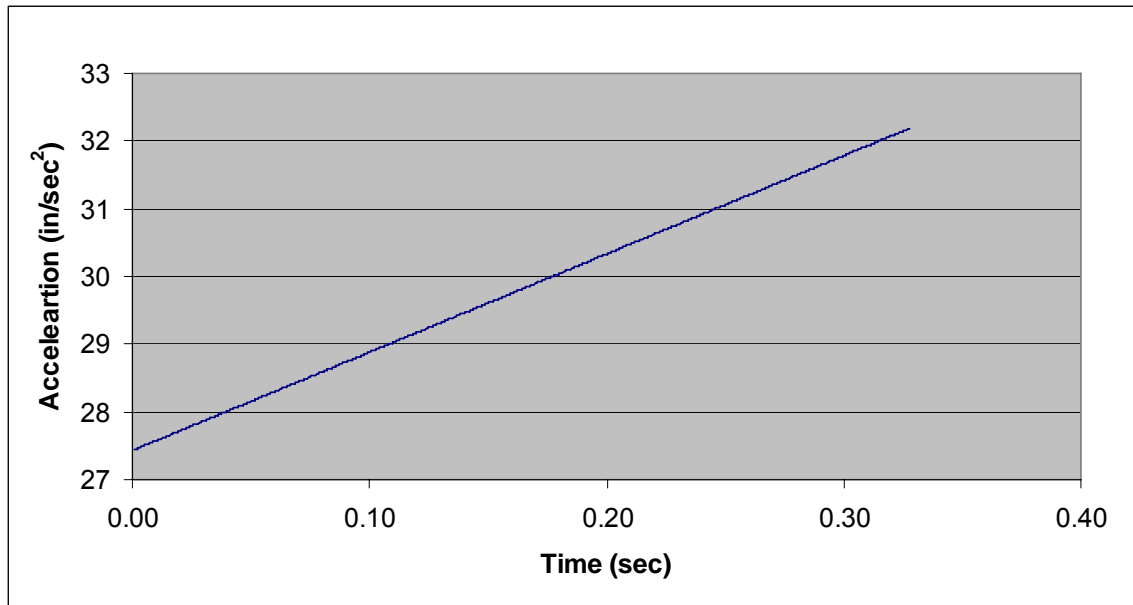


Figure 4-1. Linear acceleration of rammer during T-180 fall.

Thus, a third-order equation was used to determine the impact velocity of the rammer at the time of impact. Impact velocities were thus calculated from the laser displacement data and compared to the impact velocities measured using the photo gate mounted on the compaction mold base plate. The results of this T-180 test configuration showed a mean impact of 14.19 ft-lb with standard deviation of 0.24 as measured by the displacement laser. The photo gate mean kinetic energy was 14.30 ft-lb with a standard deviation of 0.99. The results from this test show fairly poor agreement between the two measurements. These discrepancies are due to the distance between the emitter and detector optical fibers as well as the difficulty in precisely aligning the sensors. Since the mold and appurtenances limit the installation height to 6 inches, and to bypass the issue with the rammer being perpendicular to the photo gate and its signal being missed, the sensors were then relocated to the top of the compactor. Now, the time that the rammer breaks the line of sight of the detector and the time that the line of sight is restored is

used. The only line of sight of each other, for both sensors, is when the rammer is in contact with the impact pad (Figure 4-2).

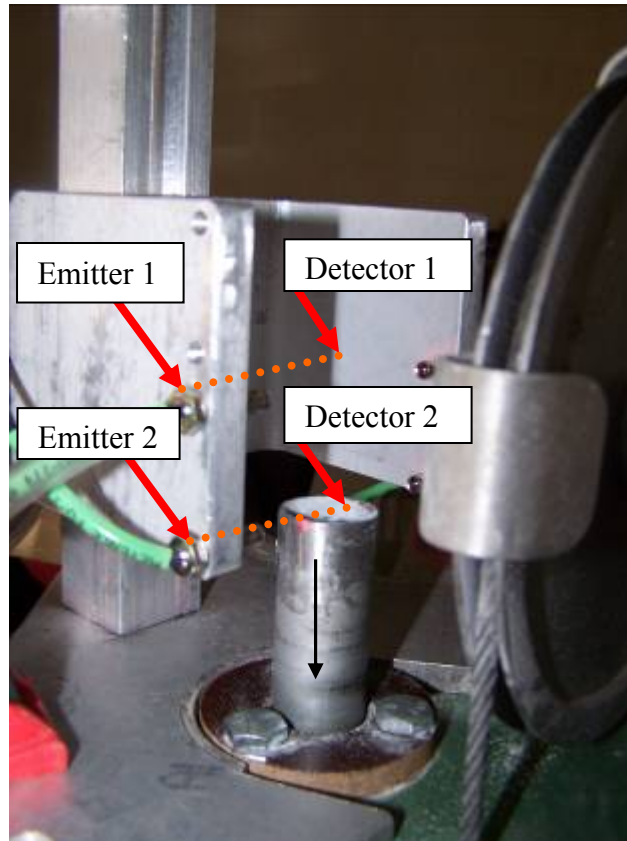


Figure 4-2. Sensor alignment on compaction machine.

This setup was verified to operate correctly 100% of the time regardless of the orientation of the rammer. The verification study was performed again using the laser displacement record and the velocity of impact measured by the photo gate. The test operated for five complete rotations, and all 48 impacts were recorded by both sensors. A third-order polynomial derivative to describe the impact velocity of the rammer was compared to the velocity measured with the photo electric gate. This testing configuration resulted in much better agreement than the base mounted configuration. These results have been summarized in terms of the rotation of the

hammer as well as in terms of the entire population of rotations. However, for the summary of all rotations, it is important to note that the first rotation has been removed from the data set due to the improper function of the photo gate during this initial test run (Table 4-1).

Table 4-1. Summary Statistics for Validation Study Hammer Rotations

		Velocity Measured Using Photo Electric (in/sec)	V_{imp} Laser (in/sec)	Kinetic Energy Measured (ft*lb)	Kinetic Energy Calculated (ft*lb)	Potential Energy Measured (ft*lb)	Percent Difference between Kinetic Measured and Calculated (%)	Percent Difference Between Kinetic Measured and Potential Measured (%)
Rotation 1	Average	114.24	115.84	14.09	14.48	15.27	2.73	7.77
	Standard Deviation	0.70	0.81	0.17	0.20	0.07	0.55	0.97
Rotation 2	Average	115.85	115.76	14.48	14.46	15.28	-0.16	5.19
	Standard Deviation	0.66	0.60	0.17	0.15	0.04	0.68	1.12
Rotation 3	Average	115.73	115.65	14.46	14.43	15.29	-0.15	5.44
	Standard Deviation	0.63	0.63	0.16	0.16	0.04	0.63	0.90
Rotation 4	Average	115.82	115.61	14.48	14.42	15.30	-0.37	5.35
	Standard Deviation	0.79	0.87	0.20	0.22	0.03	0.67	1.32
Rotation 5	Average	115.91	115.95	14.50	14.51	15.30	0.07	5.27
	Standard Deviation	0.86	0.78	0.22	0.20	0.06	0.73	1.26
All Impacts in Rotation 2-5								
All Impacts in Rotation 2-5	Average	115.83	115.74	14.48	14.46	15.29	-0.15	5.31
	Standard Deviation	0.72	0.72	0.18	0.18	0.04	0.67	1.12

Note: With the removal of the data acquired from the first rotation of the rammer, the summary statistics of the population are based on 39 impacts.

This table illustrates the precision in the measurement of mean velocity for each rotation of the rammer. The mean impact velocity measured using the photo electric gate was within 0.21 in./sec of the actual impact velocity of the rammer as measured by the displacement laser. This is less than a 0.2% difference. This maximum difference in measured velocities thus resulted in a maximum percent difference in the mean energy calculations of 0.37 ft-lb while the other three useable rotations resulted in an absolute percent difference of less than 0.16 ft-lb.

As an additional step to verify the accurate measurement of the impact energy, attention focused on the standard deviation of the rammer’s impact energy for each rotation. Analysis

shows there to be good agreement between the standard deviation of the energy of each individual rotation as well as for the population as a whole for each rotation of the hammer.

From this study it was verified that the velocity measured using the photo electric sensors mounted on the top of the compaction machine at a spacing of 0.950 inches is sufficiently accurate to establish the velocity at impact of the compaction rammer, as well as the variance of the energy during operation.

4.2 Accuracy of the Instrument

In an effort to verify that the Keyence M1H photo electric sensors accurately measure the velocity of a passing object, a time study was performed that utilized the operational frequency of the sensors and the distance between them. The design distance of the sensors was set at 0.950 inches. For an AASHTO T-180 compaction test, Newtonian physics shows that for a free fall of exactly 18 inches, an impact velocity of 117.89 inches per second should result. This velocity was then used to determine the time required for the rammer to travel a distance of 0.950 inches or approximately 0.00806 seconds.

The operational frequency of the M1H photo electric sensors is 50 kHz (50,000 samples per second). This means that every $1/50,000^{\text{th}}$ of a second, the sensor outputs a voltage corresponding to its line of sight. This results in an accuracy of 0.00002 seconds in the detection of the rammer at either sensor. Thus, for a two-sensor system, the precision in the time of travel measurement could be off by a maximum of 0.00004 seconds.

In order to determine the effect a time of travel error of 0.00004 seconds might have, this tolerance was applied to the 0.00806 time determined previously. A maximum error was found to result in an impact velocity range of 117.28 to 118.45 inches per second. This translates into a

range in energies from 14.84 to 15.14 ft-lb, resulting in a tolerance of $\pm 1\%$ of the actual energy for a single impact.

It should be noted that this is the maximum error for any given impact. This error in time determination is considered random error and could thus occur for either sensor, translating into ± 0.00002 seconds and the mean centered about 0 seconds. As such, as long as multiple impacts are being measured, any error is offset when taking the average of the values.

4.3 Validation of the Testing Procedure

4.3.1 Photo Electrics

The next step in the validation of the photo electric sensor was to validate the testing procedure. The same data that was used in the sensor validation study was used. However, now that it has been verified that the photo electric velocity measured was valid for use as the impact velocity, only these values were utilized. A bootstrap analysis was performed for each hammer rotation in an effort to verify that the mean energy for a single rotation of the hammer was representative of the mean of the multiple rotations of the machine. In addition, the variance of a single rotation of the rammer was representative of the variance of the machine.

For this analysis, the mean energy for each rotation was found to be the mean of the bootstrap for all cases. In comparison to the mean, the variance of the bootstrap was found to be small and in all cases less than 0.0024. Since this value was small and the mean of the sample was equal to the mean of the bootstrap, statistically, the mean for any single rotation is representative of the mean of the machine.

In an effort to validate the variance of the mean energy for a single hammer rotation, the bootstraps for each rotation were again utilized. The bootstrap mean variance for a single

rotation was compared to the variance of the energy for each rotation and found to be within ± 0.01 of the variance of the rotation.

The next step was to take all 39 impacts and use a bootstrap to randomly select 10 of 39 impact samples. This task was performed 4,000 times and each time the mean of the bootstrap and the variance of the bootstrap were calculated. The mean variance of the 39 bootstrap values was compared to the actual variance for each rotation of the hammer. In this case, the difference between the bootstrapped variance and the variance of each single rotation of the hammer was again found to be within ± 0.01 of each other. This indicates that the variance of a single rammer rotation is sufficient to establish the variance of the machine to $\pm 0.01 \text{ ft}^2\text{-lb}^2$.

4.3.2 Compliance Instrumentation

In an effort to ensure the repeatability of the results of the load cell and accelerometer base compliance device, several tests were run at UF and FDOT's SMO. These tests consisted of placing the compaction mold base plate in the compactor, using the standard base plate vise. Several impacts were then created on the face of the load cell and recorded.

The data generated by the impacts were then plotted as load and acceleration with respect to time. The results of these tests showed the ease of accurate repeatability for a given machine (Figures 4-3 and 4-4). This is due primarily to the accuracy under which these instruments have been calibrated.

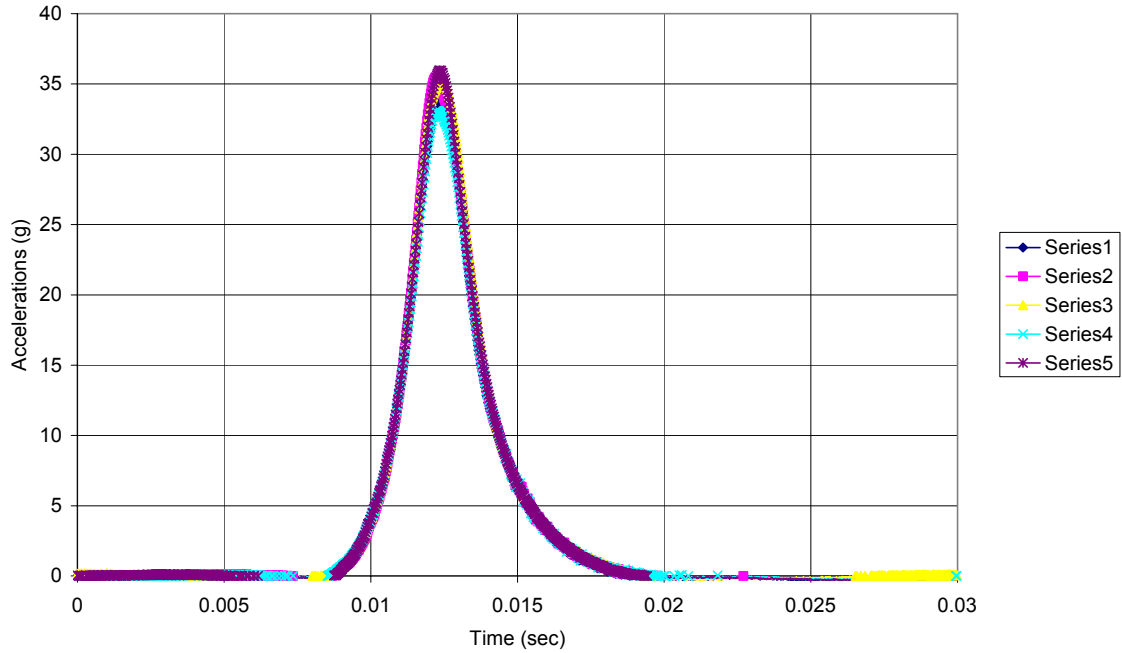


Figure 4-3. Typical acceleration and time duration plot for base compliance measurement.

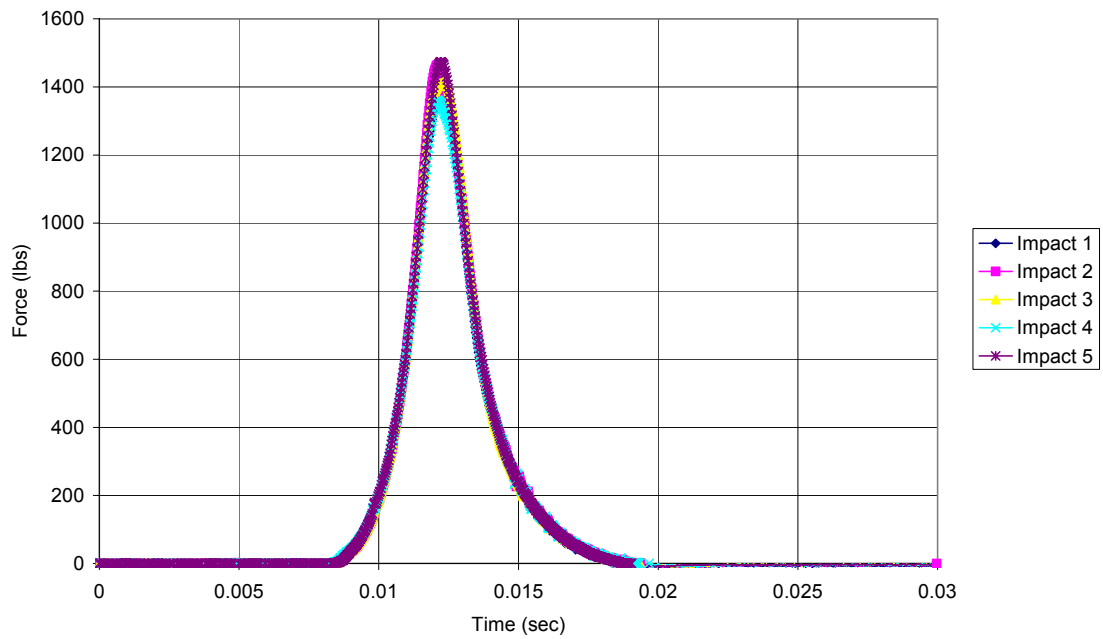


Figure 4-4. Typical force and time duration plot for base compliance measurement.

CHAPTER 5
LABORATORY TESTING AND DATA ANALYSIS

5.1 PDEC Setup Description

Use of the portable dynamic energy calibrator (PDEC) relies on two main components, the photo electric gate and a base system compliance mold. The photo electric gate pictured in Figures 5-1 and 5-2 easily mounts on the top of the compactor using two C-clamps. Adjustment to the photo electric gate then needs to be performed to ensure that the velocity is measured across the last 0.950 inches of travel or just prior to the rammer's impact on the impact pad. This can be done by loosening the adjustment thumb bolts on the back of the mounting post (Figure 5-2) and sliding the "C" channel section vertically until sensor pair 2 is at its switching point (see Figure 5-3 as well as Figure 4-2 in Section 4.1 and Appendix A).

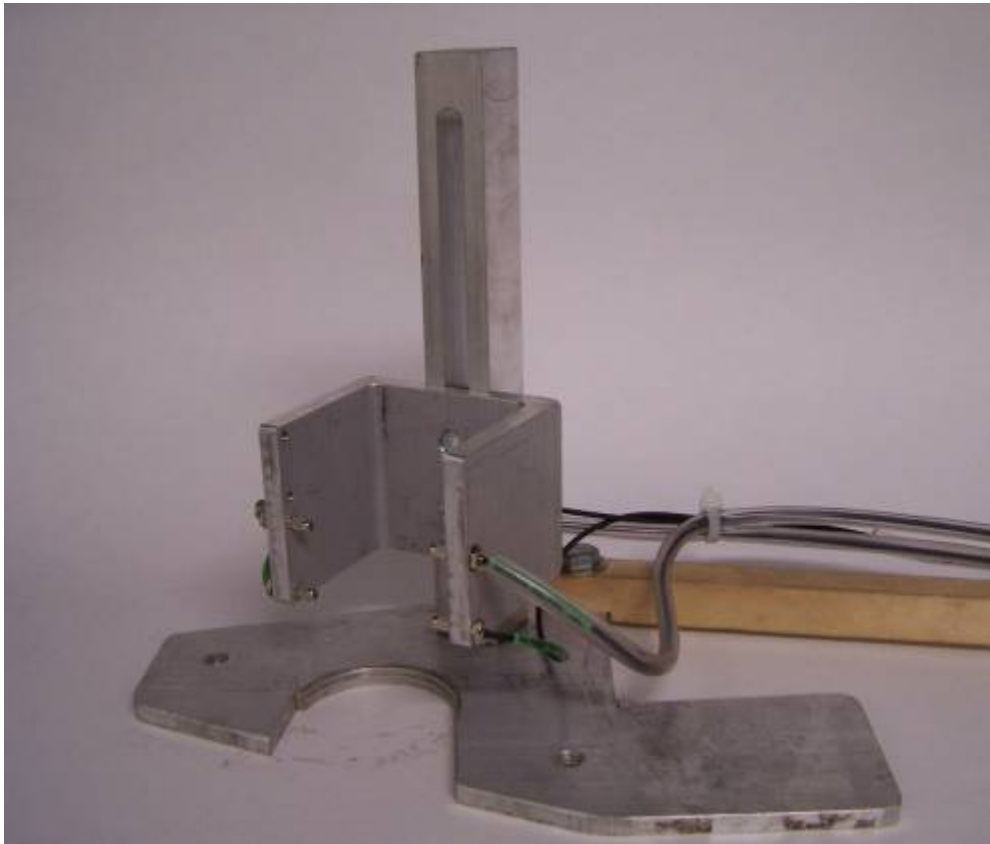


Figure 5-1. Photo electric gate – Front view.

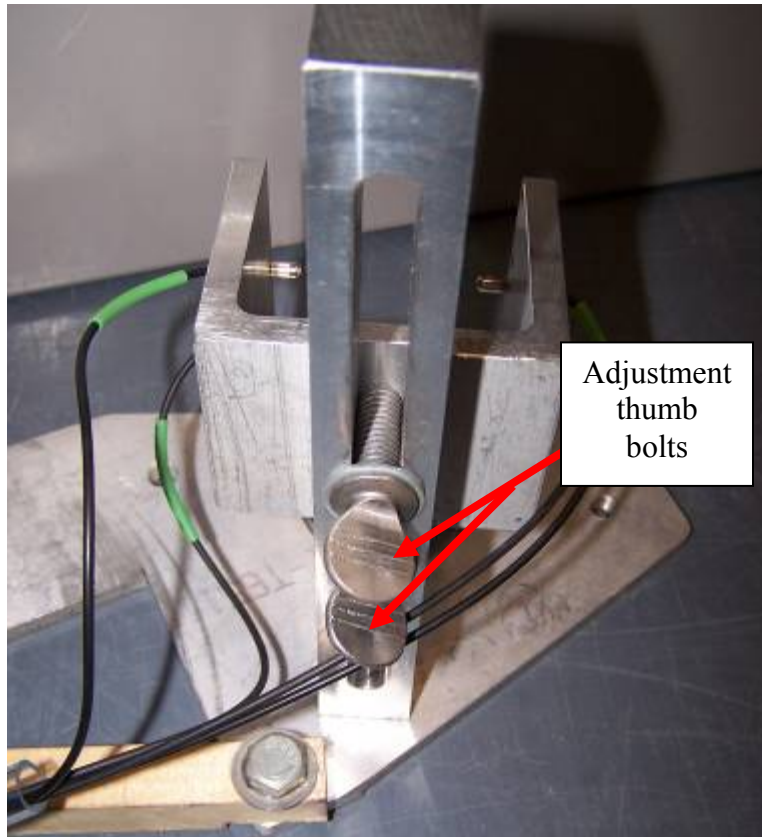


Figure 5-2. Photo electric gate – Rear view.

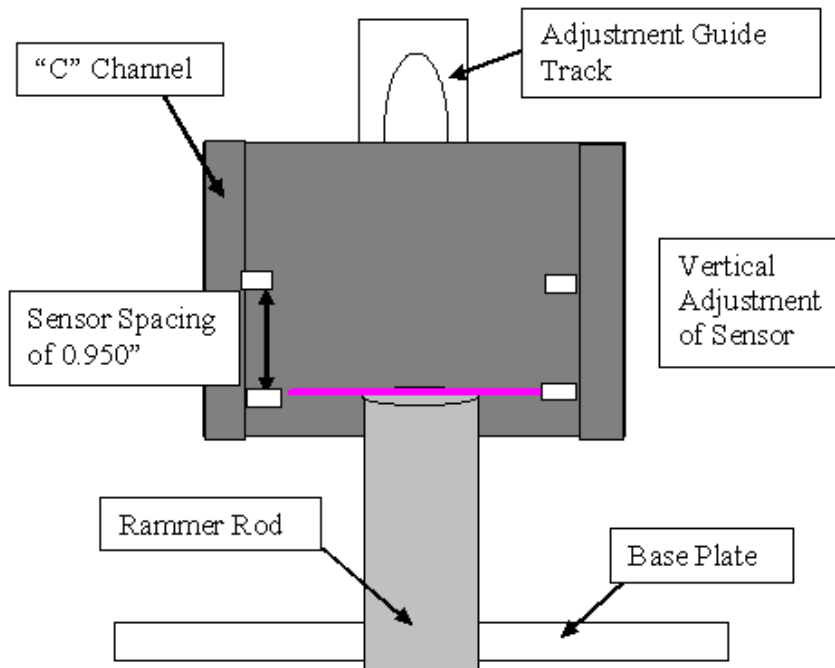


Figure 5-3. Illustration of rammer rod at switching point of sensor 2.

With the plywood and sorbothane impact pad in place, the compaction machine can be started. The digital output from the Keyence M1H photo electric sensors are simultaneously sampled by a Measurement Computing 1608H data acquisition system at a rate of 50,000 samples per second (50 kS/s) and the laptop converts it to the impact velocity of the rammer (Figure 5-4). Since the rammer mass (including the rod) was determined at the time of testing, by measuring the impact velocity, the kinetic energy of the rammer for each impact was calculated.

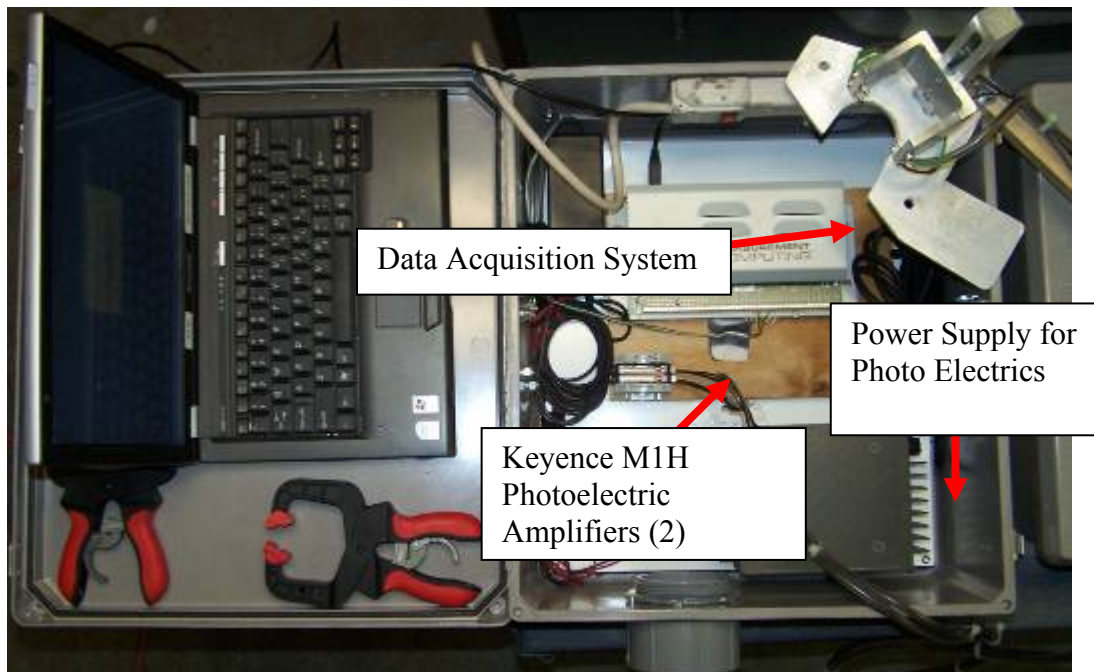


Figure 5-4. Data acquisition system setup and sensors.

Following the velocity measurements, forces and accelerations from a single rammer impact are measured at the base of the compactor (Figure 5-5). The device is stationary and there is a single impact location, so the rammer must be positioned correctly to impact the force sensor. Figure 5-6 shows an instrumented 4-inch mold assembly with a force impact sensor and

500-g accelerometer affixed to the base. The respective mold assembly, 4-inch or 6-inch (not shown), is placed into the compactor and used to measure single impact forces and accelerations.

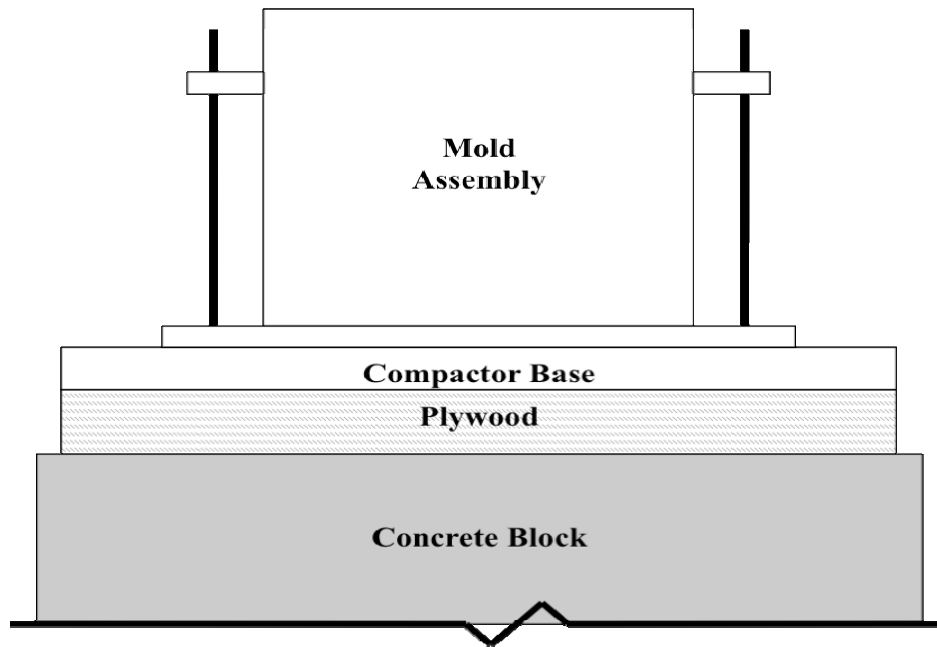


Figure 5-5. Base system configuration with mold assembly.

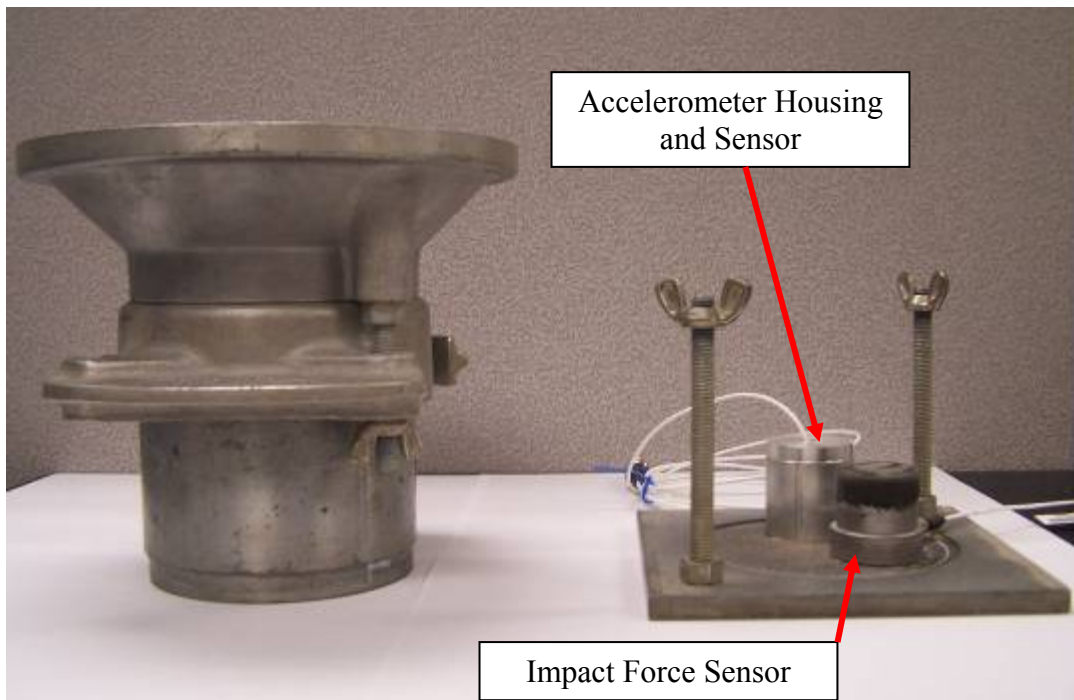


Figure 5-6. Instrumented mold assembly.

The force sensor is positioned such that contact is made with it at the centroid of the rammer.

The accelerometer is located two inches away from the force center, center-to-center. The sensor instruments are connected to the portable data acquisition system/notebook PC for data sampling (40,000 samples per second (40 kHz)) and storage.

5.2 Testing Program Overview

The PDEC was taken to 16 state and independent compaction laboratories in Florida for testing on T-99 and T-180 mechanical compactors. Laboratories were identified per FDOT districts as ones certified to perform T-99 and T-180 tests. Districts 2, 5, and 7 (see Figure 5-7) were visited.

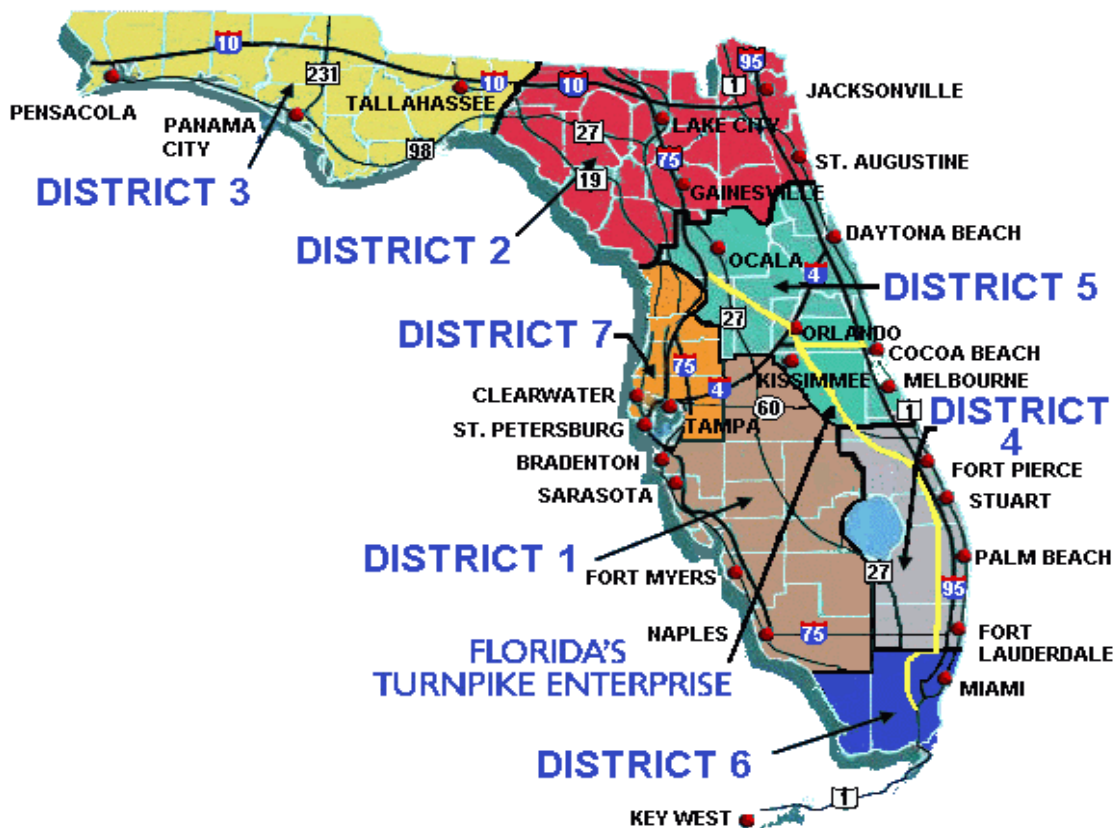


Figure 5-7. FDOT district map.

The data obtained provided a sample population with summary statistics, such as the mean, median, and standard deviation in impact velocity (function of drop height), kinetic energy (function of mass and impact velocity squared), and compliant characters (peak force, peak acceleration, peak time). The Modified (T-180) Proctor configuration was most frequently encountered in the laboratories. Thirty T-180 compactors and four T-99 machines were tested. The compactors were set on a foundation of cast-in-place concrete or block with aluminum, steel or plywood cushions between the machine base and the foundation (Figures 5-8 and 5-9). The results and analysis presented are from the thirty T-180 compactors.

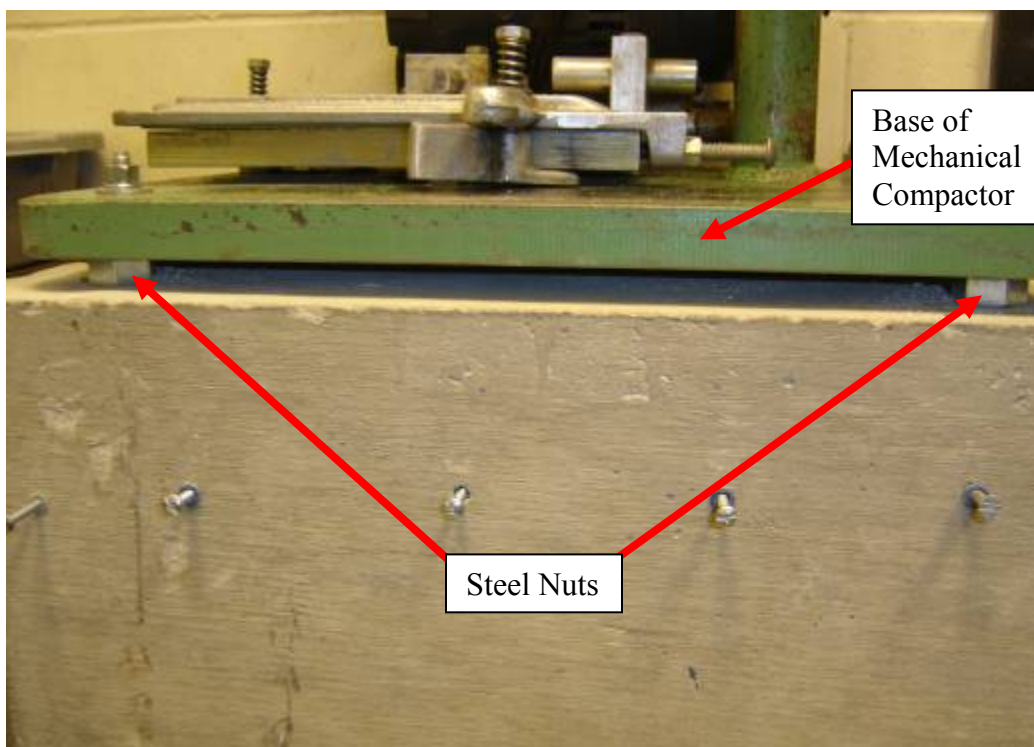


Figure 5-8. Compactor foundation with steel cushion.



Figure 5-9. Compactor foundation with plywood cushion.

5.3 Testing Results and Analysis

5.3.1 Kinetic Energy Assessment

Impact velocity was measured for each machine. The kinetic energy of each impact is calculated from the impact velocity and rammer mass of each machine as shown in Equation 1-2. The kinetic energy data was summarized for the variance per machine and variance among all the machines by considering the mean per machine. Figure 5-10 presents the frequency distribution of the mean energy of the sample population. The mean energy is taken as the sum of all kinetic energies in a single round of rammer impacts (8-10 impacts) divided by the number of impacts and represents a single machine.

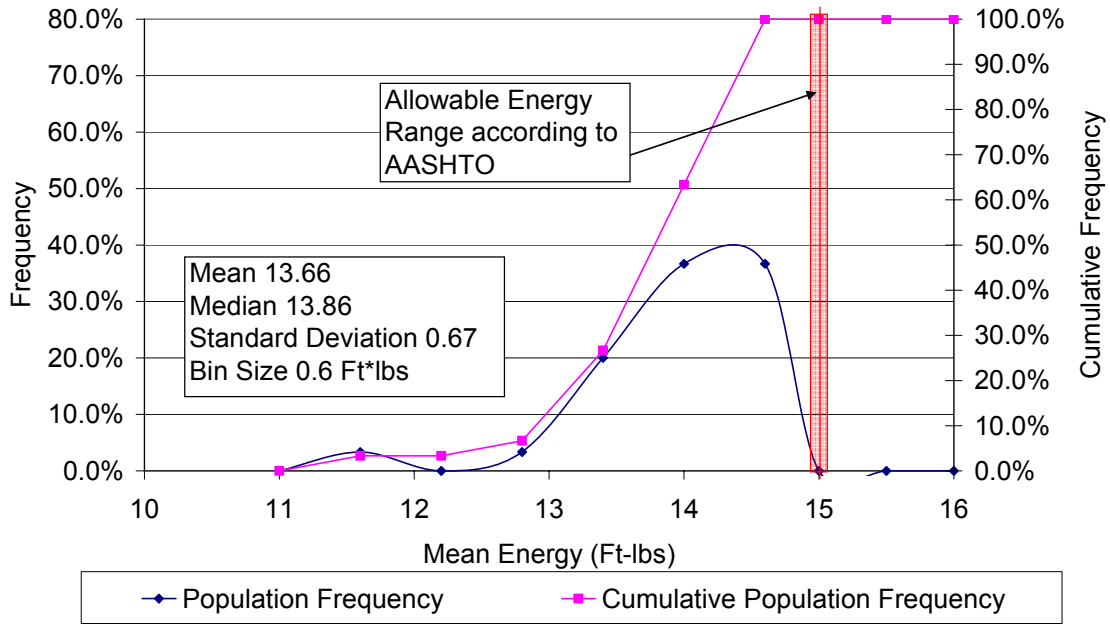


Figure 5-10. Frequency distribution of mean energy data.

A bootstrapping procedure was then performed to ensure that the sample was representative of the entire population of machines. The functionality of bootstrapping is a numerical simulation by re-sampling real data. The process of bootstrapping takes the values of the sample population and randomly selects a value a specified number of times to generate a single bootstrap. From those values randomly selected, summary statistics can be used to describe the characteristics of that bootstrap, namely the mean and variance. In an effort to ensure enough repetition in the bootstrap procedure, 4,000 bootstraps were generated. The mean of all 4,000 was then calculated as well as the variance and mean of the bootstrap variances. These summary statistics for the bootstraps are then used to make statistical inferences for the entire population. In order to verify that the sample is sufficient to represent the population, two key values are analyzed: the variance of the bootstrap variances; and the mean variance of the bootstrap. As long as the variance of the bootstrap variances is small, it indicates that enough samples were taken from the population to establish the variance of the bootstrap population accurately. In this

case, the mean variance of the bootstraps can then be compared to the variance of the sample population. Good agreement of these values indicates the sample is representative of the population.

From the sample of thirty machines, a bootstrap analysis was performed on thirty values (with the possibility of repetition) randomly chosen to generate each bootstrap. From the summary statistics, the mean of the variance for all of the bootstraps is 0.43. When compared with the variance of the sample population (which had a variance of $0.45 (.067^2)$), it is apparent they are in excellent agreement. This shows that the population sample of thirty machines is representative of the entire population of proctor compaction machines. Next, the variance of the bootstrapped variances was calculated to be 0.03. Since it is significantly smaller than the mean variance of the bootstraps, it shows there is high accuracy in the determination of the variance of the population using those thirty machines.

Also using the bootstrap method, one is able to gain more confidence in the distribution of the data collected. The bootstrap procedure quantifies the uncertainty of the mean through statistical inference. Shown in Figure 5-11 is the frequency distribution of the bootstrap procedure for the 30 mean energy data values. The distribution type suggested by Figure 5-11 is normal with a mean and median very close to that of the sample population (13.66 ft-lb and 13.86 ft-lb, respectively). The distribution of the variance of the data mean is small ($0.3^2 = 0.09$). A comparison of the data and bootstrap distributions show good agreement. It is important when comparing the bootstrap distribution and the data distribution for one to note the summary statistics, to see if the mean energies coincide and the median values are close to one another. For example, the median value for the bootstrap is within 1.5% of the median value for the laboratory data set.

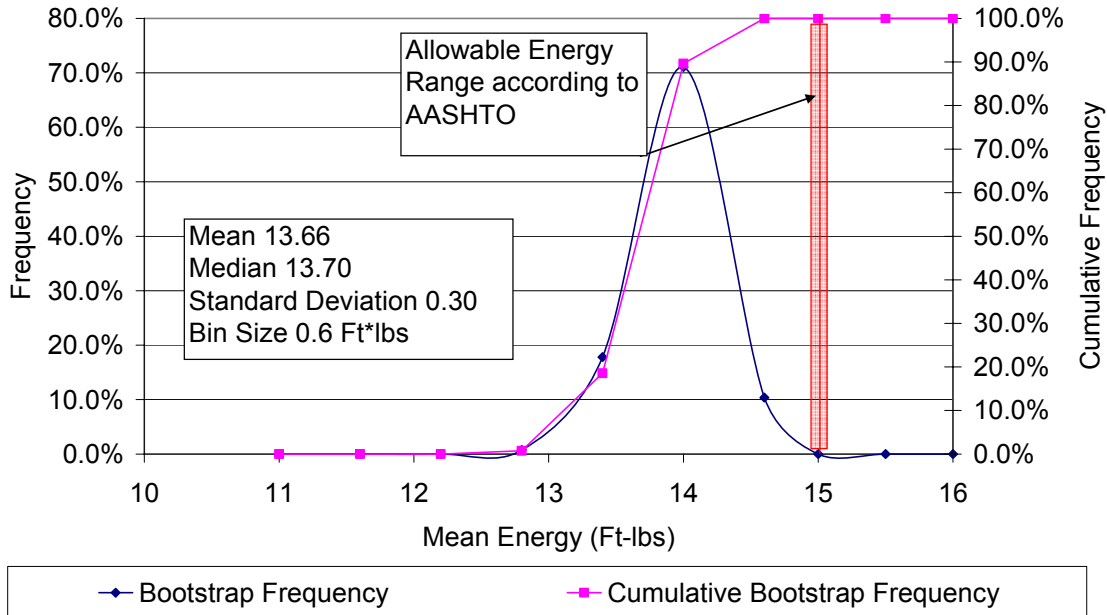


Figure 5-11. Bootstrap frequency distribution of mean energy.

Figure 5-12 shows the frequency distribution of all the calculated kinetic energies from the data; these are not a representation of the mean values. These are all energies for a single round of impacts on each machine. Compared to Figure 5-10, Figure 5-12 provides better insight into the percent of the population below the allowable range of energy based on AASHTO standards of rammer mass and drop height. Through close examination and interpretation of Figure 5-12, it is possible to see that the cumulative frequency portion of the plot showed no impacts above the AASHTO specified energy. Rammer masses were measured for each machine and it was observed that all rammer masses were within the specified tolerances. This indicates that low energy available for compaction stems from low impact velocities.

Frequency Distribution of Each Impact for 1 Hammer Rotation
(30 Machines)

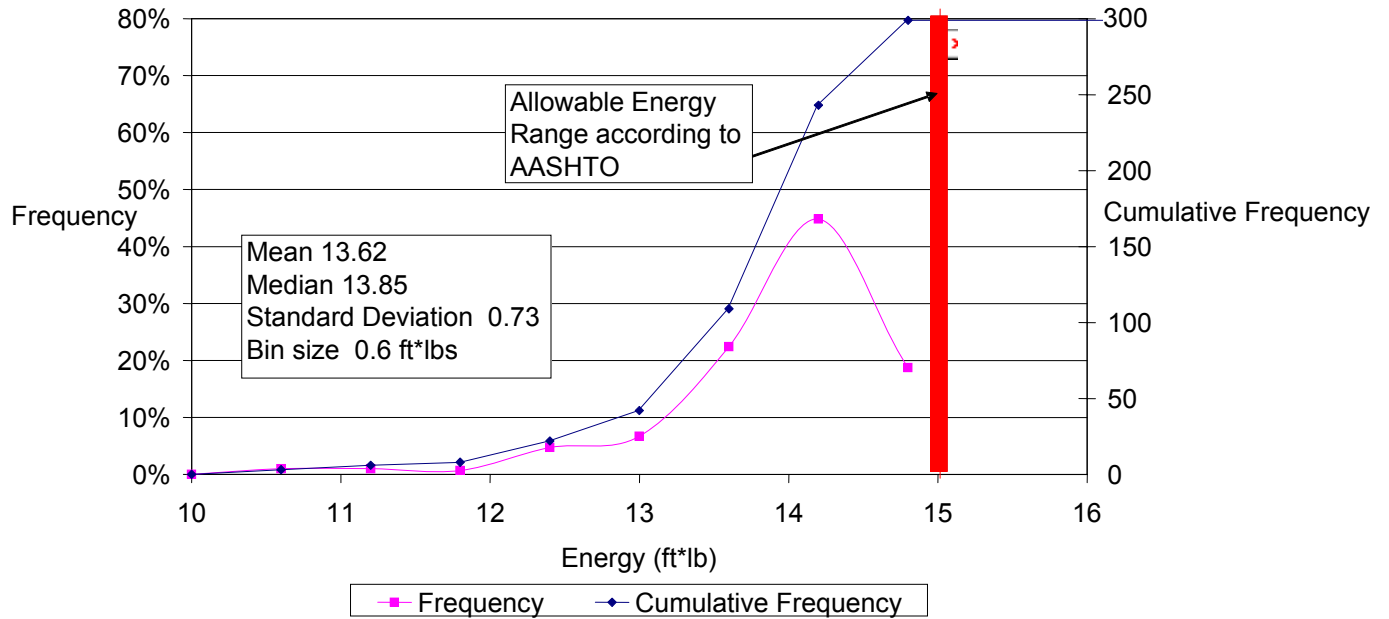


Figure 5-12. Frequency distribution of all energy data.

With the summary statistics and the mean velocity and energy, Figures 5-13 and 5-14 were generated as scatter plots. In this case, a scatter plot provides a good visual identification of machines which may be outliers of the population and where to look for the sources of error. For example, in Figure 5-13, there is an extreme outlier with a standard deviation of approximately 4.5 and mean velocity of 103 inches/second. Since the velocity, V , is a function of the drop height and free fall acceleration ($V=\sqrt{2g\Delta h}$), this indicates there is a problem with the machine not consistently dropping the mass from the same height and/or large inconsistent frictional impedance during the free fall acceleration. A point near the low end of the standard deviation, for example 0.5, indicates a consistent deviation about the mean for this machine, essentially showing that the drop height and or the frictional forces on the rod are consistent for each fall of the rammer. According to drop heights in AASHTO and ASTM standards, the range of allowable velocities based on free fall is shown in red in Figure 5-13.

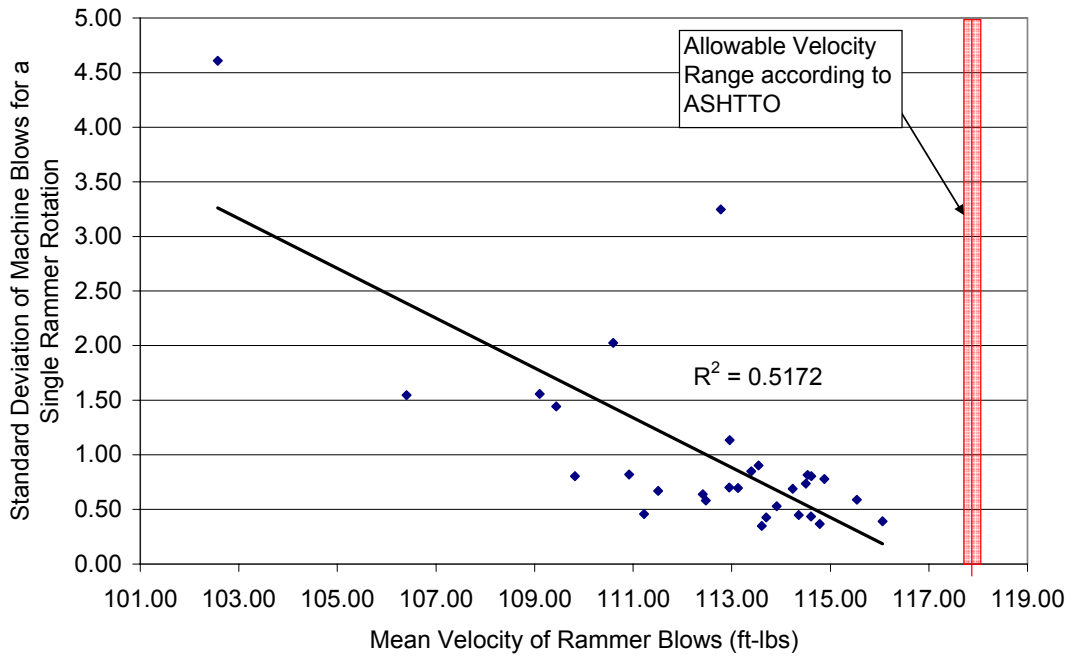


Figure 5-13. Scatter plot of energy standard deviation versus mean velocity.

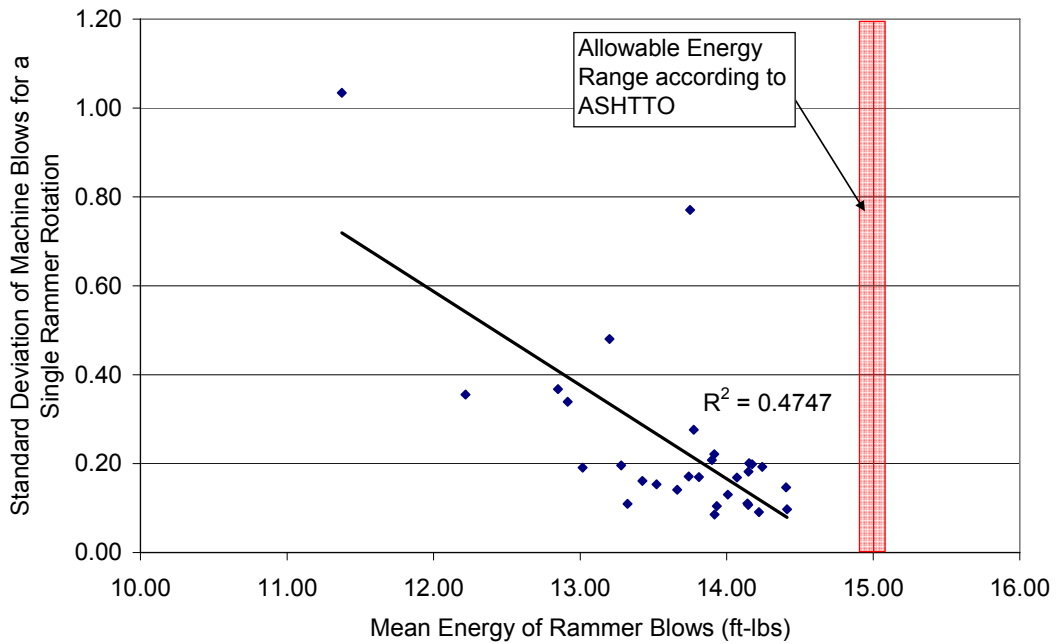


Figure 5-14. Scatter plot of energy standard deviation versus mean energy.

Figure 5-14 shows the scatter plot for the mean kinetic energy of the sample population. The results show a definitive trend in the data. That is to say, machines that display a low standard deviation in the energy delivered by each blow are more likely to have a higher mean energy, whereas machines that have a large energy standard deviation typically have a lower mean energy associated with the machine. In general, the majority of the population has small standard deviations (≈ 0.10 to 0.20) and all are below the range of allowable energy according to the AASHTO standards T-180.

5.3.2 Manual Compaction Rammer

In order to establish a baseline for understanding the kinetic energy measurements from the mechanical compaction machine, testing was performed to quantify the typical kinetic energy available from a T-180 manual rammer.

Six manual T-180 compaction rammers were tested. Three of the six were different commercial models. The rammers were attached to a temporary frame using C-clamps to maintain vertical alignments (see Figure 5-15). The photo electric gate was then attached to an adjustable height table and the plywood and sorbothane impact pad placed beneath the impact point of the rammer.

The adjustment described for the mechanical compactor was performed for this setup as well, i.e., the sensors were set such that the rammer was located just beyond the switching point. The mean of at least 25 impacts were then recorded for each of the six manual T-180 rammers. These six means were then summarized by their mean and variance, $14.25 \text{ ft}\cdot\text{lb}$ and $0.005 \text{ ft}^2\text{-lb}^2$, respectively, and then used to perform a bootstrap procedure to ensure sufficient tests were conducted. The bootstrap mean was calculated as $14.25 \text{ ft}\cdot\text{lb}$ as well, with the mean variance of the bootstraps determined to be $0.004 \text{ ft}^2\text{-lb}^2$. The most probable reason why the theoretical

energy of 15 ft-lb (10 lb x 1.5 ft drop height) was not achieved is due to friction between the rammer and hammer housing. It is virtually impossible to provide a friction free fall since even a slight inclination of the hammer will create concomitant friction between the moving mass and its housing.

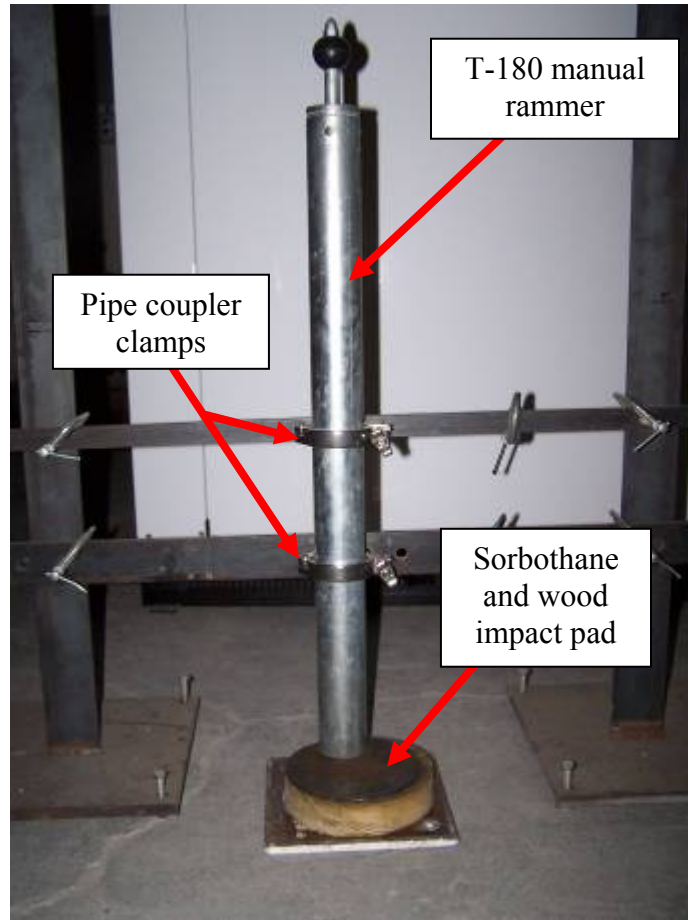


Figure 5-15. Frame for maintaining vertical alignment of rammer.

Of significant importance with the bootstrap procedure is the variance determined to be on the order of 6×10^{-6} , which indicated that the calculation of the bootstrap means is highly precise. This high precision indicates that six values for the energy associated with the manual compaction rammer is a sufficiently large population to accurately determine the mean and variance to describe the population of all T-180 manual rammers. The small variance suggests that for any manual rammer, the energy is likely to be extremely close to 14.25 ft-lb.

5.3.3 Base Compliance

Following the measurement of the kinetic energy for each of the machines tested at the sixteen compaction labs, force and acceleration at the base plate were measured for multiple impacts of the rammer (three to eight) on each machine in the population using the base compliance instrumentation (Figure 5-6). The mean force and acceleration for each machine were plotted and reflect similarly to each other for any given machine (Figures 5-16 and 5-17), machines with a high mean force display high mean accelerations. The standard deviations are relatively low compared to the magnitudes, although there are four types of base systems in the population and measurements are also a function of velocity.

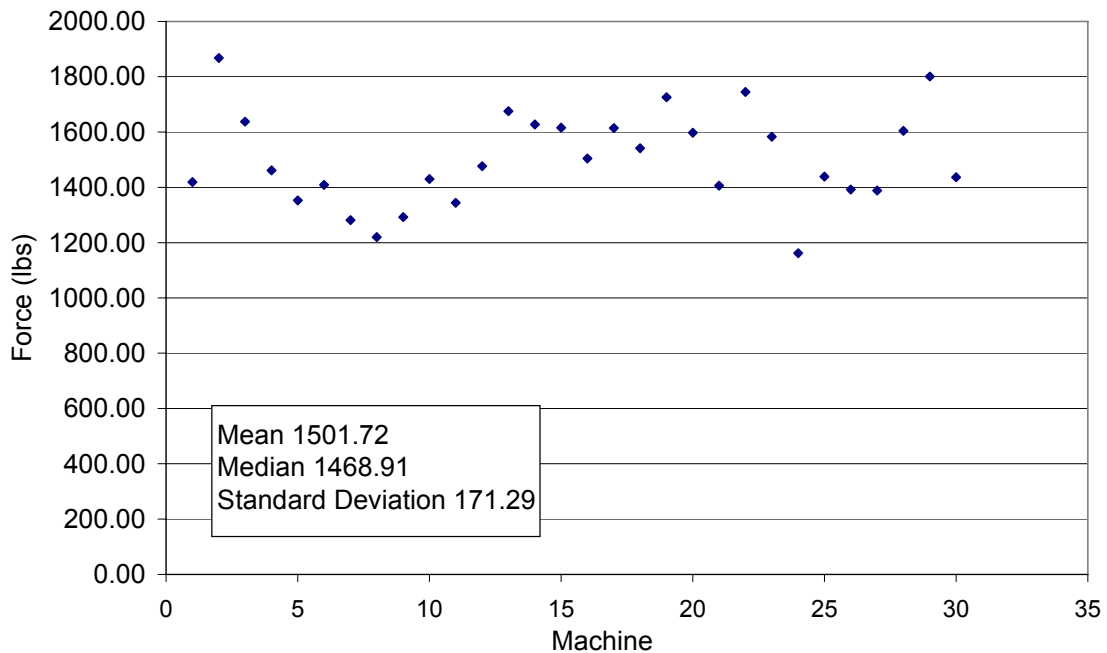


Figure 5-16. Scatter plot of average maximum force.

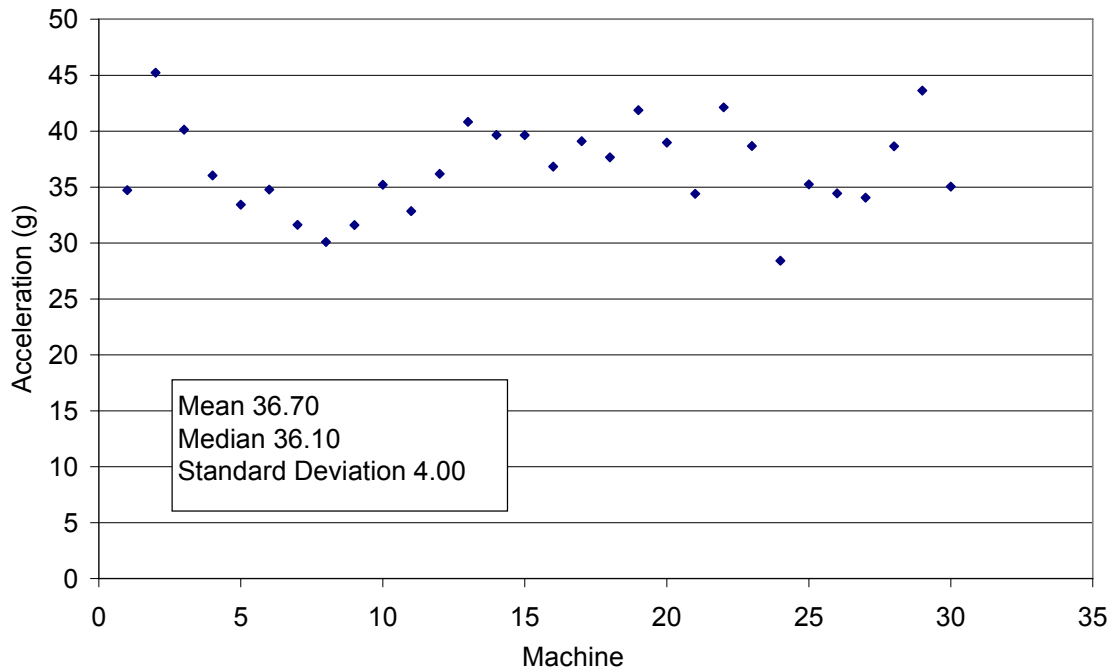


Figure 5-17. Scatter plot of average maximum acceleration.

The primary reason for measuring the force and acceleration at the base of the compaction equipment was to quantify the energy or the purpose of identifying a possible source of difference in compaction density results. As previously discussed, the stiffness of the material supporting material beneath the compaction mold has an influence on the resulting maximum dry density and optimum moisture content.

5.3.4 Force Compressive Energy Theory

In an effort to quantify the effect that different base types have on the compaction process, the energy at the base of the compaction device needed to be quantified. Compressive energy at a point along a Standard Penetration Test (SPT) rod can be expressed as an integral of the force squared with respect to time multiplied by the dynamic impedance of the SPT rod (Palacios 1977) (Equations 5-1 and 5-2). In the case of the load cell being the same cylindrical shape and displaying 1-D wave transmission down the length of the cylinder (the load cell housing in this

case), the same assumptions hold true and validate the use of SPT compressive energy equations in this study.

$$\text{Dynamic Impedence} = \frac{c}{Ma} \quad (5-1)$$

$$\text{Energy}_{\text{impact}} = \frac{c}{Ma} \int_0^t F_i^2 \quad (5-2)$$

where C = wave velocity (in./sec)

M = Young's Modulus (psi)

A = cross sectional area (in.²).

5.3.5 Compressive Energy Results

For each machine, a numeric integral of the force squared was calculated for each load cell impact record and recorded for the time over which it occurred. The mean of the integrals were then recorded for each machine (Appendix B).

The calculation of the dynamic impedance of the load cell was not able to be determined directly. However through a reverse model using the magnitude of the integral of the force squared, it was determined that the dynamic impedance of the load cell is on the order of 1/300 ft/(sec-lb) . Through utilization of the back-calculated dynamic impedance of the load cell, energies were able to be thus calculated and used to establish the variance of energy in population of bases.

Due to the difference in the wave transmission through the different sized compaction mold base plates required for the T-180A and T-180B tests (4 inch and 6 inch diameter molds), the sample population of base compliance data was subdivided by base type for further analysis. This resulted in a subpopulation of nine T-180A machines and twenty-one T-180B machines. The subpopulation of the T-180A machines was too small to be used in further calculations.

Of the twenty-one T-180B machines, several different base types were represented. These consisted of two machines with plywood mounted between the machine and the foundation block, three machines mounted directly to concrete, and the remaining sixteen machines were mounted with aluminum spacers or steel nuts between the machine and their foundation blocks. The integral of the force squared as well as the maximum force and maximum accelerations for machines mounted with plywood displayed uncharacteristically high compliance measurements. Due to this unrepresentative behavior and uncommon occurrence in the population (two machines), they were removed from the final analysis so as to not misrepresent the sample population of T-180B compaction machines.

Summary statistics were performed on the compressive energies of the nineteen machines as well as a bootstrap procedure to ensure that the population of nineteen machines was adequate for quantifying the variance of the population. A summary table containing the measurements from the nineteen machines is presented in Table B-2 in Appendix B. The mean compressive energy was 11.66 ft-lb with a variance 1.39 (ft-lb)^2 and the mean of the bootstrap means was 11.65 ft-lb and variance mean of the bootstraps equal to 1.32 (ft-lb)^2 . The variance of the bootstrap variances was then calculated as 0.082, more than two orders of magnitude smaller than the variance of the sample, thus indicating that nineteen machines is large enough to establish the mean and variance of the population of T-180B base compliances. The coefficient of variation (COV or CV defined in Equation 5-3) was then calculated for both the sample and bootstrap populations, and were found to be in good agreement, i.e., 0.12 and 0.11, respectively.

$$\text{COV or CV} = \sigma/\mu \quad (5-3)$$

where σ = standard deviation
 μ = mean.

After reviewing the data, it was found that the acceleration records from the base compliance impacts were not useful in determining the compressive energy characteristics at the base of the compactor. The raw measurements did display high and low values that agreed well with the force measurements, essentially verifying that the load cell was operating correctly. Since these measurements did not prove useful in the determination of energy at the base, the use of the accelerometer in the final base compliance device is not necessary for the quantification of energy.

CHAPTER 6 CONCLUSIONS AND RECOMMENDATIONS

The objective of this research was to develop a portable electronic calibration device for use on mechanical Proctor compaction machines. This equipment was successfully developed and used to quantify both the kinetic energy and the compressive impact energy on T-180 mechanical compaction machines. The results from this study provided useful insight into the variability of compaction machines, both individually and as a population.

6.1 Calibrator Conclusions and Recommendations

After performing companion monitoring with the laser displacement sensor and the photo electric gate, it was determined that the velocities measured using the photo gate are representative of the impact velocity of the rammer and can be used in kinetic energy calculation with an accuracy of $\pm 1\%$. Additionally, it was found that a single rotation of the compaction rammer is sufficient to establish the mean kinetic energy and the variance, or standard deviation, of kinetic energy for a machine.

Through the use of a dynamic load cell placed at the base of the compaction machine and capturing the impact compressive force, compressive energy can be determined. It was shown that the base system, i.e., cushion type, foundation type, influences the compressive energies and that there are large variances among the nineteen machines used for density testing. Thus, the compressive energy at the base of the system can be used for comparison among mechanical compaction machines.

The portable dynamic energy calibrator (PDEC) is easily transportable and can be readily employed in a compaction laboratory. The photo electric gate is adjustable and affixes to the top of the compaction machine with no alterations needed to the machine. The dynamic force device is placed in the compactor and captures single rammer blows. A data acquisition system, which

accompanies the devices, samples the sensors and stores the data for immediate analysis. The user can run a macro on the data collected and, with a few variables entered, can observe the rammer kinetic energy and base compressive energy.

6.2 Data Analysis Conclusions and Recommendations

On an individual basis, it was found that machines that display high variance in the kinetic energy of successive impacts tend to display low mean kinetic energies. On a population scale, it was found that all compaction machines suffered from frictional losses during the free fall of the rammer, thereby resulting in low kinetic energies. The population of manual T-180 rammers displayed higher kinetic energies than the mechanical compaction machines, suggesting frictional effects are less. Additionally, it was found that the population of manual compaction rammers has a very low variance in kinetic energies between rammers.

Due to the complexities and differences in the test setups, it was found that the compressive energy measurements were not sufficient by base type to analyze each separately. However, it was determined that the population of machine base compliances was large enough to be analyzed as a whole. Using this analysis, it was found that the COV of the compressive energy at the base of the compaction machine was much larger than that of the kinetic energy of the machines.

6.3 Conclusions

In conclusion, the portable electronic calibration device has been successfully developed and is applicable for quantifying both kinetic and compressive energy and has been used to establish the mean energy and COV for each of the two types of energy calculations for the population of T-180 compaction machines used in various soil labs in Florida. It is expected that FDOT will continue to use this equipment in the future and develop procedures to verify that all compaction machines are in compliance with appropriate standards.

LIST OF REFERENCES

- American Association of State Highway Transportation Officials (AASHTO). *AASHTO Standard Test Methods*. “T 87-86 Dry Preparation of Disturbed Soil and Soil Aggregate Samples for Test”; “T 99-01 Moisture Density Relations of Soils Using a 2.5 kg (5.5 lb) Rammer and a 305 mm (12 in.) Drop”; “T 180-01 Moisture Density Relations of Soils Using a 4.54 kg (10 lb) Rammer and a 457 mm (18 in.) Drop”; “T 88 Particle Size Analysis of Soils.”
- American Society for Testing and Materials (ASTM). *ASTM Standard Test Methods*. “D 2168-02a Calibration of Laboratory Mechanical Rammer Soil Compactors.”
- Clinch, J. R. (2006). “Soil Compaction: A Comparison of Standard Proctor and Modified Proctor Tests.” Honors Thesis. Department of Civil and Coastal Engineering, University of Florida, Gainesville.
- Das, B. M. (2002). *Principles of Geotechnical Engineering*. 5th ed. Pacific Grove: Brooks/Cole. pp. 100-117.
- Dubose, L. A. (1952). “Evaluating Taylor Marl Clay for Improved Use in Subgrades.” *Texas Engineering Experiment Station Research Report 35*. Texas A&M College. March.
- Halliday, D., Resnick, R., and Walker, J. (2000). *Fundamentals of Physics*. 6th ed. New York: Wiley.
- Palacios, A. (1977). “The Theory and Measurement of Energy Transfer During Standard Penetration Test Sampling.” Ph.D. Dissertation. Department of Civil Engineering, University of Florida, Gainesville.
- Proctor, R.R. (1933). “Description of Field and Laboratory Methods.” *Engineering News Record*. September 7, pp. 286-289.
- Ray, P. N., and Chapman, T. G. (1954). “British standard compaction test for soils: study of some factors affecting test results.” *Geotechnique*. Vol. 4 (4), December, pp. 169-177.
- Sebesta, S., and Liu, W. (2007). *Improving Calibration and Quality Control of Proctor-Style Laboratory Compaction*. Transportation Research Board, July.
- Sherwood, P. T. (1970). “The Reproducibility of the Results of Soil Classification and Compaction Tests.” *RRL LR 339*. Road Research Laboratory. pp. 27-37.
- Texas Department of Transportation (TexDOT). “Laboratory Compaction Characteristics and Moisture Density Relationship of Base Materials.” *TexDOT-113-E*.

APPENDIX A

OPERATION OF INSTRUMENTATION

The following steps are critical to the functionality of the Portable Electronic Calibration Device.

The Photo Electric Gate

- Assemble the guide post and base plate of the photo electric gate. The opening in the guide post is perpendicular to the leading edge of the base plate.
- Remove the thumb bolts from the “C” channel containing the photo electric sensors.
- Place the “C” channel on the guide post such that the line of sight of the photo electric sensors is parallel to the base plate’s leading edge. The orientation of the “C” channel should be such that the photo electric sensors are on the bottom side of the “C” channel. Refer to the “C” channel for determining top/bottom of channel for proper orientation.
- Thread the thumb screws through the guide post and into the back of the “C” channel and lightly tighten.
- Mount the photo electric assembly on the compaction machine such that the rammer guide rod and guide rod bushing fall within the radius cut in the base plate and the base plate is clear of all moving parts.
- Use quick connection clamps to fasten the base plate to the top plate of the compaction machine. Making certain the clamps used for mounting will not interfere with the moving parts of the compaction machine.
- Check the rotational alignment of the photo electric sensors to ensure that the guide post is in proper orientation such that the lenses of the photo electric sensors will not be struck by the rammer rod.
- Turn on laptop and insert the USB cable for the measurement computing Data Acquisition system into any USB port on the laptop.
- Turn on power strip in instrumentation box.
- Turn on AC to DC power converter making certain to not change the voltage setting. (Voltage should be set at approx 13V).
- Allow sufficient time for Data Acquisition and instrumentation to warm up and stabilize approximately 20 minutes.
- In the mean time select the appropriate size impact pad for the machine configuration to be tested. Place the impact pad on the compaction machines base and clamp in place using the mold clamp for the machine.

- Note: Two impact pads have been provided and have been adequate for the testing performed by the University of Florida. The purpose of the impact pad is to provide a safe surface for impact of the rammer and dampen the blow of the rammer such that the rammer is in at rest before being lifted by the rammer. Should a particular machine display instances in which the rammer is picked up by the grabber during a bounce following the previous impact changes to the impact pad must be made to eliminate this effect. However the impact pad should have sufficient rigidity such that there is little deflection or deformation when the rammer is at rest on the surface of the impact pad.
- Place the rammer face on the impact pad.
- From the top of the machine adjust the vertical alignment of the “C” channel. The line of sight of the bottom pair of sensors should be just slightly above the top of the rammer rod so that the time of impact can be recorded. The switching threshold can be observed by watching the lights on the photo electric amplifiers change from green to red. Lift the rammer rod slightly to ensure that the amplifier switches in all orientations of the rammer this will ensure that the impact energy can be measured for all impacts.
- From the desktop of the provided laptop open TracerDAQ Pro.
- With “Strip Chart” selected from the list of options click “Run”.
- On the file menu select “load configuration” and choose “User0.”
- Make certain the fiber optic cables of the instrumentation stay clear of the rammer and grabber assembly during monitoring.
- Select the “Play” button on the top of the screen. This will begin the acquisition of data from the photo electrics.
- Turn the compaction machine to the on position and record one complete revolution of the rammer.
- Once the rotation is complete switch the compaction machine off.
- Select the “Stop” to end the acquisition of data.

Saving and Importing Data into Excel

- From the file menu of TracerDAQ Pro select “Save As.”
- Change the file type to “.txt” and save the record of impacts in the directory of your choice.
- From the desktop open Microsoft Excel 2003.

- From the file menu select “Open.” On the File type drop down select “All Files.” Navigate to the file that was just recorded. Select it and choose “Open.”
- The “Import Text Wizard” will be opened within excel, select delimited and choose “Next.”
- Select “Comma” as a delimiter and click “Next.”
- Click “Finished.”
- Now The Data is ready for automated processing.

Kinetic Energy Processing

- On the keyboard of the laptop press the control key and the “y” at the same time.
- Fill in the cell requiring the mass of the rammer after verifying its mass.
- Table generated now displays the kinetic energy of each impact of the rammer.
- The photo electric sensors can now be removed from the top of the compaction machinery.

Compliance Measurement Setup and Testing

- Thread the load cell into the hole specified on the base plate of the compaction mold with the stem of the load cell in the final placement as marked.
- Gently thread the coaxial instrumentation cable supplied onto the stem of the load cell. Using the open BNC connector on the ICP, connect the load cell.
- Turn on the PCB ICP.
- Allow the load cell and ICP to warm up and stabilize.
- Place the compaction mold into the compaction machinery and clamp in place using the base plate clamp for the machine.
- Align the rammer such that when the machine is switched on it will impact the load cell squarely on the impact surface. The resting height of the rammer face should be on the same horizontal plane as the face of the load cell and the grabber for the machine in its lowest point of travel and gripping the rammer rod.
- When the machine is switched on the rammer will begin to be lifted, rotate approximately 35-45 degrees and freefall. Attention to the location to the impact should be checked. Upon verifying the rammer will impact squarely testing is ready to be performed.

- On the File menu of TracerDAQ Pro select “Load Configuration,” select “User2” profile.
- Press the play button to begin recording.
- Switch the machine to the on position momentarily and return it to the “off” position immediately after the rammer has been dropped, successive impacts of the rammer could damage the load cell or the rammer face. It is imperative that only one impact occur at a time and that it occur squarely on the load cell face.
- Realign the rammer for the next impact again this alignment will be approximately 35-45 degrees from the load cell face. Following the alignment steps outlined above.
- Switch the machine on for a single impact. Continue repeating rammer alignment and turning the machine on for a single impact on the load cell face until at least 3 impacts have been recorded.
- Follow the same steps presented in the segment about saving and importing the data into excel.

Compliance Energy Processing

- On the keyboard of the laptop press the control key and the “x” at the same time. This begins the automated data processing of the compressive energy.
- The table generated from this data displays the compressive energy from each of the impacts recorded. The variance of these values is directly related to accuracy of the rammer alignment. The mean is reported and representative of the machine as long as proper care was taken by the operator to align the rammer properly before switching the device on.

APPENDIX B
LABORATORY DATA

Table B-1. T-180 Rammer Rotation Summary Statistics Per Machine

Machine Number	Rammer Mass (lbs)	Velocity (in/sec)			Kinetic Energy (ft-lb)		
		Mean	Median	Standard Deviation	Mean	Median	Standard Deviation
1	10.00	110.59	110.98	2.02	13.20	13.29	0.48
2	10.00	110.92	110.98	0.82	13.28	13.30	0.20
3	10.00	112.96	113.10	1.14	13.78	13.81	0.28
4	9.98	114.61	114.46	0.44	14.15	14.11	0.11
5	10.02	114.36	114.46	0.45	14.14	14.17	0.11
6	10.00	113.12	113.37	0.70	13.81	13.87	0.17
7	9.98	111.22	111.24	0.46	13.32	13.33	0.11
8	9.99	114.24	114.18	0.69	14.07	14.06	0.17
9	10.00	102.57	100.42	4.61	11.37	10.88	1.03
10	10.00	114.61	114.73	0.80	14.17	14.20	0.20
11	10.01	111.51	111.76	0.67	13.43	13.49	0.16
12	10.00	114.79	115.01	0.37	14.22	14.28	0.09
13	10.00	114.54	114.73	0.82	14.15	14.20	0.20
14	10.00	113.54	113.37	0.90	13.92	13.87	0.22
15	10.00	113.91	114.18	0.53	14.01	14.07	0.13
16	9.99	113.61	113.64	0.35	13.92	13.92	0.09
17	9.99	113.70	113.64	0.43	13.93	13.92	0.10
18	10.00	109.82	109.95	0.81	13.02	13.05	0.19
19	10.02	113.40	113.50	0.85	13.90	13.92	0.21
20	10.00	114.50	115.01	0.74	14.15	14.28	0.18
21	9.98	112.95	112.83	0.70	13.74	13.71	0.17
22	9.99	109.44	109.70	1.44	12.91	12.97	0.34
23	10.01	112.47	112.56	0.58	13.66	13.68	0.14
24	10.00	115.54	115.57	0.59	14.41	14.41	0.15
25	10.00	109.10	108.94	1.56	12.85	12.81	0.37
26	10.00	106.40	106.50	1.55	12.22	12.24	0.36
27	10.01	112.78	113.64	3.25	13.75	13.95	0.77
28	10.00	114.88	115.15	0.78	14.24	14.31	0.19
29	9.92	116.06	115.85	0.39	14.41	14.36	0.10
30	9.92	112.41	112.56	0.64	13.52	13.56	0.15

Table B-2. T-180B Base Compliance Summary Per Machine

Machine Number	Average Integral of Force ² (lbs ² -sec)	Base Mounting	Compressive energy (ft-lbs)
1	3686.23	Direct to Concrete	12.29
5	3533.44	Direct to Concrete	11.78
6	3672.25	Direct to Concrete	12.24
7	3176.89	Aluminium Spacer	10.59
9	3260.51	Aluminium Spacer	10.87
10	3381.72	Aluminium Spacer	11.27
11	3104.20	Aluminium Spacer	10.35
12	3691.42	Aluminium Spacer	12.30
15	4213.78	Aluminium Spacer	14.05
16	3393.28	Steel Spacer	11.31
18	3491.33	Aluminium Spacer	11.64
19	3774.38	Steel Spacer	12.58
20	3863.64	Steel Spacer	12.88
21	3433.66	Aluminium Spacer	11.45
23	3934.11	Aluminium Spacer	13.11
24	2566.72	Aluminium Spacer	8.56
26	3492.05	Aluminium Spacer	11.64
27	3334.38	Aluminium Spacer	11.11
30	3465.89	Steel Spacer	11.55

Note: Does not include plywood base mounting.

APPENDIX C

RAMMER HEAD TESTS

A study of the rammer head surface shapes and the impact stresses was proposed to address the bearing failure during the compaction process. Previous research by Clinch (2006) showed for an A-3 material under mechanical T-180 compaction, expected densities were not achieved and was attributed to the soil type and stresses from the rammer head. This was shown by a shoving of the soil during the test. Figures C-1 and C-2 illustrate the soil prior to and following compaction. It was proposed to modify the rammer head to reduce or eliminate the stress concentrations.



Figure C-1. Modified Proctor sample prior to compaction.



Figure C-2. Modified Proctor sample after compaction.

The rammer head typically used in a 6-inch mold is sector shaped (see Figure C-3(a)). Although, due to the possible stress concentrations at the apex of the rammer surface, a double sector shape rammer (see Figure C-3(b)) is available from Rainhardt and was purchased for research. The Texas Department of Transportation (TexDOT) suggests using this rammer on material that is difficult to compact (TexDOT-113-E, Sect. 6). With the double sector rammer, the stress concentrations were believed to be mitigated. This can be explained. During impact, as the stresses from each apex permeate into the soil, the high concentrated lateral stresses act equal and opposite, thereby totaling zero. Tests were performed in an attempt to quantify stress distributions across the surface of the rammer as well as the effect of the rammers on soil density for A-2-4, A-1-b, and A3.

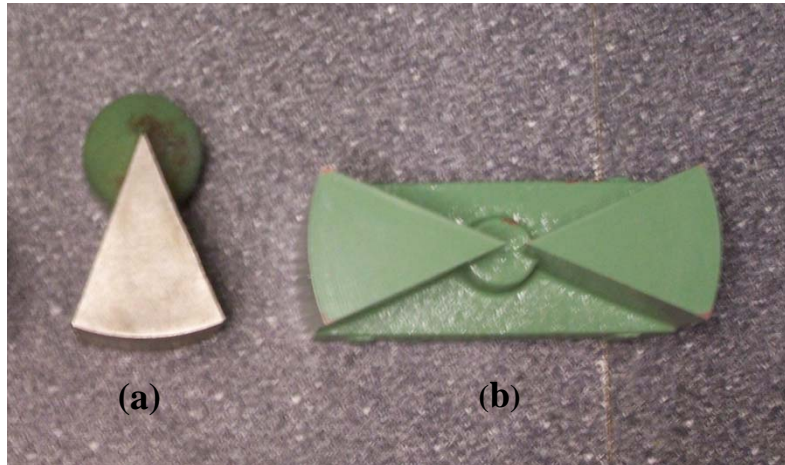


Figure C-3. Sector rammer heads: (a) single; and (b) double.

The researchers used Pressurex pressure indicating film to quantify stress distributions over a surface area. The film was placed on top of a sorbothane impact pad situated in the mechanical compactor. The maximum stresses for a single impact of rammer (a) was captured and sent for analysis. Figure C-4 shows the stress distribution over the surface of the single sector rammer, the lowest stresses being the dark purple and the highest the yellow to red or a difference of 40 to 60 psi. These results did not provide an indication of a stress concentration at the apex, but did suggest the highest stresses occurred along the edge nearest the apex.

Compaction tests using the single and double sector heads (Figure C-3) on typical embankment soils (A3, A-1-b, A-2-4) were performed. The purpose of the tests was to determine differences in densities between compaction with the two different shape rammers and to develop a methodology for use of the double sector head, if required. Soils were obtained and identified according the AASHTO specifications at the State Materials Office (SMO) in Gainesville, Florida. The tests with the double sector head were conducted according to the same standard as the single sector head. For example, 5 layers, 56 blows per layer, 10-lb rammer, and drop height of 18 inches were used.

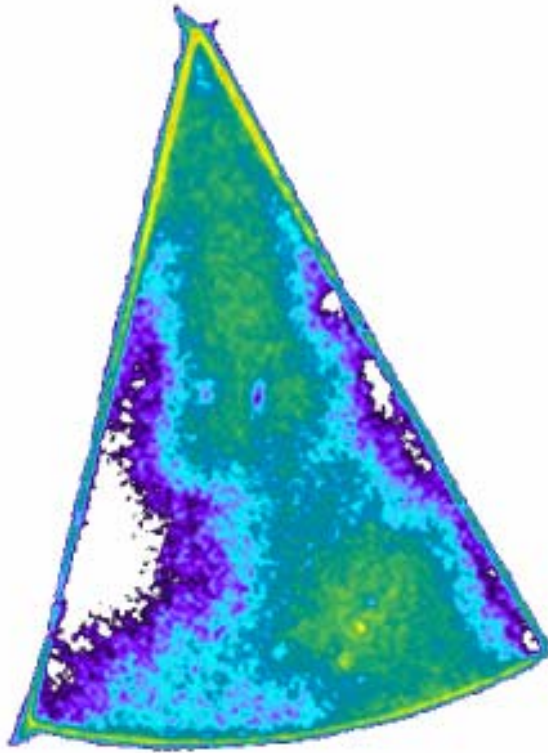


Figure C-4. Pressure scan image results of single sector head.

Figure C-5 shows the typical Proctor curve from a T-180 modified compaction test on each of the soils. Three of these tests were performed for each soil type with the single sector head. A direct comparison of the mean value of five dry densities obtained at or near optimum moisture content, for each soil, is shown in Figure C-5. The dry densities for the branch (A-2-4) and coastal (A3) soils appear to agree well, while the agreement for the Florida rock soil does not.

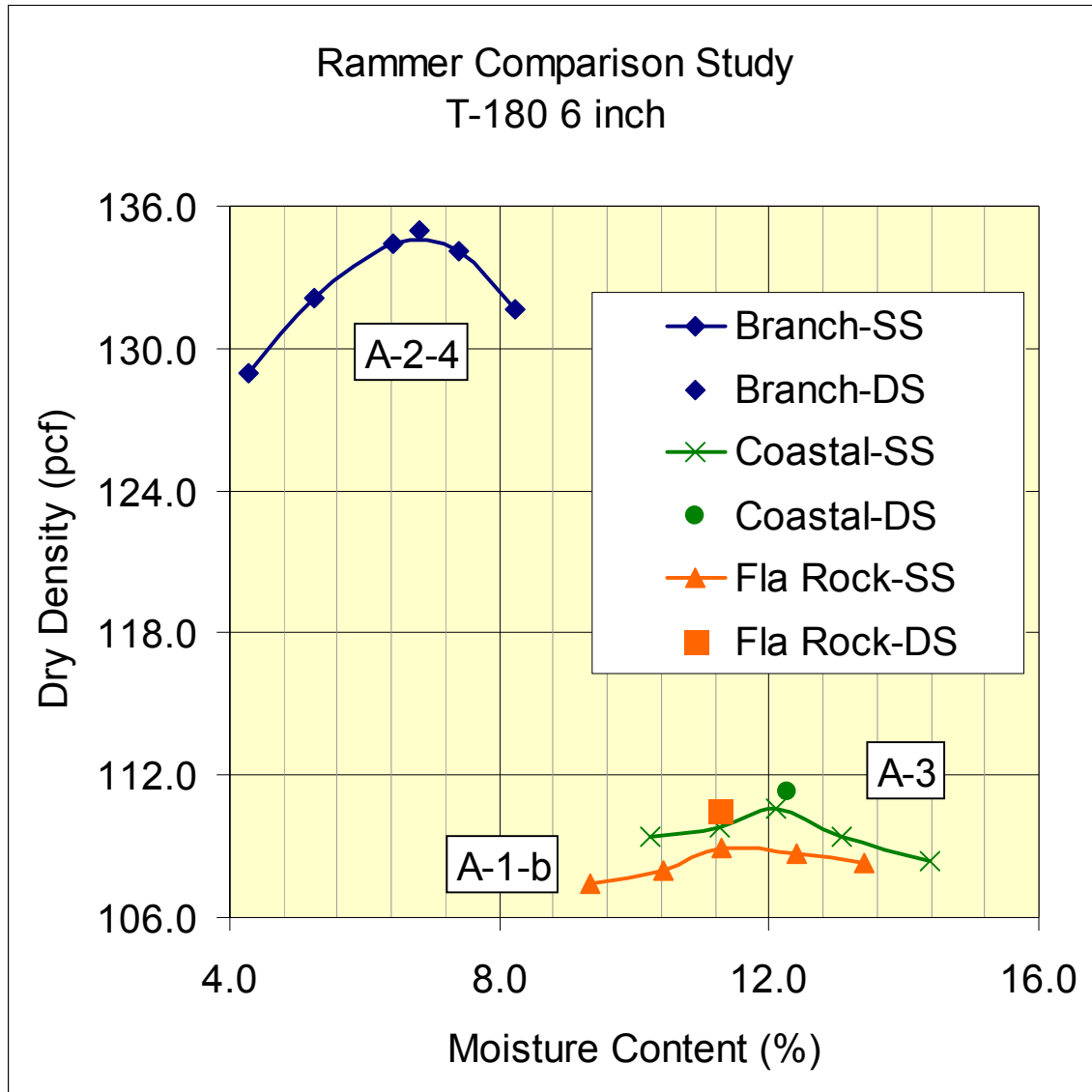


Figure C-5. Average compaction results of branch, coastal, Florida rock soils.

Table C-1 presents the summary statistics for the tests on each soil type. Only a complete summary is provided for the tests performed with the double sector, as only three single sector tests were performed. Complete test results are presented in Appendix D. All tests with the double sector head had low coefficients of variation, suggesting small scatter of the data around the mean or confidence in the repeated test procedure. The percent differences for all soils are

within a 1.5% margin. ASTM D-2168 standard calibration procedures allow for an absolute difference in maximum dry densities from consecutive manual versus mechanical tests of 2.0%.

Table C-1. Summary Statistics of Density Results

	Maximum Soil Density					
	Double Sector Rammer			Single Sector Rammer		
	Branch (A-2-4)	Coastal (A3)	Fla Rock (A-1-b)	Branch (A-2-4)	Coastal (A3)	Fla Rock (A-1-b)
Mean, μ (pcf)	134.96	111.34	110.5	134.59	110.6	108.94
Stdv, σ (pcf)	0.1855	0.1497	0.1673			
COV	0.0014	0.0013	0.0015			
Percent Difference (%)	0.2749	0.6691	1.4320			

The limited data shows the reduction in bearing capacity failure when the double sector head is used. As the density results indicate, an acceptable agreement between the tests with the different rammer shapes also showed there was substantially less digging into the material and the material compacted well. This suggests that the presence of the additional sector, which is symmetrically oriented with the other, eliminates the high stresses that lead to bearing failure during impact.

Based on the limited number of tests conducted, it is recommended that the double sector head be used to address the bearing failure process, following AASHTO D-T180.

APPENDIX D

SOIL DENSITY RESULTS FROM RAMMER HEAD TESTS

Table D-1. Coastal Soil Densities for Single Sector Rammer

SOIL TYPE	4" T-99	MOISTURE	MOISTURE	MOISTURE	MOISTURE	MOISTURE	SOIL TYPE	4" T-180	MOISTURE	MOISTURE	MOISTURE	MOISTURE	MOISTURE
A-3* Coastal	Test # 1	9.5	10.4	11.5	12.5	13.6	A-3* Coastal	Test # 1	9.6	10.5	11.5	12.4	13.2
# 23457		DENSITY	DENSITY	DENSITY	DENSITY	DENSITY	# 23457		DENSITY	DENSITY	DENSITY	DENSITY	DENSITY
-200%: 10.8%*		108.0	107.9	108.2	108.3	108.0	-200%: 10.8%*		110.3	110.4	110.9	110.1	108.9
LL: NP							LL: NP						
PI: NP	Test # 2	MOISTURE	MOISTURE	MOISTURE	MOISTURE	MOISTURE	PI: NP	Test # 2	MOISTURE	MOISTURE	MOISTURE	MOISTURE	MOISTURE
Mach.# 5		10.6	11.7	12.5	13.4	14.4	Mach.# 1		9.7	10.2	11.4	12.3	13.2
Ht. 11.97"		DENSITY	DENSITY	DENSITY	DENSITY	DENSITY	Ht. 18.00"		DENSITY	DENSITY	DENSITY	DENSITY	DENSITY
wt. 5.50 lbs.		107.7	107.7	108.3	108.2	106.7	wt. 10.00 lbs.		109.5	110.7	111.0	110.4	109.2
Dia.: 1.989"							Dia.: 1.997"						
	Test # 3	MOISTURE	MOISTURE	MOISTURE	MOISTURE	MOISTURE		Test # 3	MOISTURE	MOISTURE	MOISTURE	MOISTURE	MOISTURE
		10.6	11.6	12.5	13.5	14.5			9.4	10.2	11.4	12.3	13.2
		DENSITY	DENSITY	DENSITY	DENSITY	DENSITY			DENSITY	DENSITY	DENSITY	DENSITY	DENSITY
		108.0	108.1	108.3	108.3	106.9			110.7	111.4	111.3	110.6	109.4
		MOISTURE	MOISTURE	MOISTURE	MOISTURE	MOISTURE			MOISTURE	MOISTURE	MOISTURE	MOISTURE	MOISTURE
	AVG.	10.2	11.2	12.2	13.1	14.2		AVG.	9.6	10.3	11.4	12.3	13.2
		DENSITY	DENSITY	DENSITY	DENSITY	DENSITY			DENSITY	DENSITY	DENSITY	DENSITY	DENSITY
	AVG.	107.9	107.9	108.3	108.3	107.2		AVG.	110.2	110.8	111.1	110.4	109.2
SOIL TYPE	6" T-99	MOISTURE	MOISTURE	MOISTURE	MOISTURE	MOISTURE	SOIL TYPE	6" T-180	MOISTURE	MOISTURE	MOISTURE	MOISTURE	MOISTURE
A-3* Coastal	Test # 1	10.1	11.2	12.2	13.4	14.0	A-3* Coastal	Test # 1	10.4	11.3	12.0	13.0	14.3
#23457 # 23457		DENSITY	DENSITY	DENSITY	DENSITY	DENSITY	# 23457		DENSITY	DENSITY	DENSITY	DENSITY	DENSITY
-200%: 10.8%*		108.6	109.0	109.5	109.4	108.4	-200%: 10.8%*		109.2	109.4	110.6	109.4	108.5
LL: NP		LBR	LBR	LBR	LBR	LBR	LL: NP		LBR	LBR	LBR	LBR	LBR
PI: NP		26	30	29	26	21	PI: NP		27	25	28	23	23
Mach.# 4							Mach.# 2						
Ht. 12.03"	Test # 2	MOISTURE	MOISTURE	MOISTURE	MOISTURE	MOISTURE	Ht. 18.00"	Test # 2	MOISTURE	MOISTURE	MOISTURE	MOISTURE	MOISTURE
wt. 5.51 lbs.		10.0	11.2	12.2	13.0	14.0	wt. 10.00 lbs.		10.2	11.3	12.1	13.1	14.6
Area: 2010.68mm		DENSITY	DENSITY	DENSITY	DENSITY	DENSITY	Area: 2000.75mm		DENSITY	DENSITY	DENSITY	DENSITY	DENSITY
		108.9	108.7	109.5	109.1	108.8			109.5	110.0	110.6	109.4	107.9
		LBR	LBR	LBR	LBR	LBR			LBR	LBR	LBR	LBR	LBR
		31	30	34	28	24			28	37	30	28	20
	Test # 3	MOISTURE	MOISTURE	MOISTURE	MOISTURE	MOISTURE		Test # 3	MOISTURE	MOISTURE	MOISTURE	MOISTURE	MOISTURE
		10.1	11.1	12.1	13.0	14.0			10.1	11.2	12.2	13.1	14.3
		DENSITY	DENSITY	DENSITY	DENSITY	DENSITY			DENSITY	DENSITY	DENSITY	DENSITY	DENSITY
		108.8	108.4	109.0	109.8	108.2			109.6	110.0	110.6	109.4	108.7
		LBR	LBR	LBR	LBR	LBR			LBR	LBR	LBR	LBR	LBR
		29	29	33	35	22			35	34	32	31	21
		MOISTURE	MOISTURE	MOISTURE	MOISTURE	MOISTURE			MOISTURE	MOISTURE	MOISTURE	MOISTURE	MOISTURE
	AVG.	10.1	11.2	12.2	13.1	14.0		AVG.	10.2	11.3	12.1	13.1	14.4
		DENSITY	DENSITY	DENSITY	DENSITY	DENSITY			DENSITY	DENSITY	DENSITY	DENSITY	DENSITY
	AVG.	108.8	108.7	109.3	109.4	108.5		AVG.	109.4	109.8	110.6	109.4	108.4
		LBR	LBR	LBR	LBR	LBR			LBR	LBR	LBR	LBR	LBR
	AVG.	29	30	32	30	22		AVG.	30	32	30	27	21

Table D-2. Spring Cemetery Soil Densities for Single Sector Rammer

SOIL TYPE	4" T-99	MOISTURE	MOISTURE	MOISTURE	MOISTURE	MOISTURE	SOIL TYPE	4" T-180	MOISTURE	MOISTURE	MOISTURE	MOISTURE	MOISTURE
A-2-4 Spring Cem.	Test # 1	7.6	8.5	9.4	10.4	11.3	A-2-4 Spring Cem.	Test # 1	6.7	8.3	9.2	10.4	11.4
# 23462		DENSITY	DENSITY	DENSITY	DENSITY	DENSITY	# 23462		DENSITY	DENSITY	DENSITY	DENSITY	DENSITY
-200%: 14.8%		114.9	115.0	116.1	116.7	115.4	-200%: 14.8%		117.7	119.6	119.7	118.2	117.0
LL: NP							LL: NP						
PI: NP	Test # 2	MOISTURE	MOISTURE	MOISTURE	MOISTURE	MOISTURE	PI: NP	Test # 2	MOISTURE	MOISTURE	MOISTURE	MOISTURE	MOISTURE
Mach #5		7.5	8.5	9.4	10.2	11.0	Mach.# 1		7.5	8.4	9.3	10.2	11.0
Ht. 11.97"		DENSITY	DENSITY	DENSITY	DENSITY	DENSITY	Ht. 18.00"		DENSITY	DENSITY	DENSITY	DENSITY	DENSITY
Wt. 5.50lbs.		115.5	115.3	116.0	116.5	115.7	wt. 10.00 lbs.		118.4	119.3	119.4	118.5	117.4
Dia: 1.989"							Dia.: 1.997"						
	Test # 3	MOISTURE	MOISTURE	MOISTURE	MOISTURE	MOISTURE		Test # 3	MOISTURE	MOISTURE	MOISTURE	MOISTURE	MOISTURE
		7.4	8.3	9.1	10.0	11.0			7.7	8.6	9.3	10.7	11.2
		DENSITY	DENSITY	DENSITY	DENSITY	DENSITY			DENSITY	DENSITY	DENSITY	DENSITY	DENSITY
		114.8	115.5	116.0	116.5	115.4			119.7	120.4	121.0	119.9	119.3
		MOISTURE	MOISTURE	MOISTURE	MOISTURE	MOISTURE			MOISTURE	MOISTURE	MOISTURE	MOISTURE	MOISTURE
	AVG.	7.5	8.4	9.3	10.2	11.1		AVG.	7.3	8.4	9.2	10.4	11.2
		DENSITY	DENSITY	DENSITY	DENSITY	DENSITY			DENSITY	DENSITY	DENSITY	DENSITY	DENSITY
	AVG.	115.1	115.3	116.0	116.6	115.5		AVG.	118.6	119.8	120.0	118.9	117.9
SOIL TYPE	6" T-99	MOISTURE	MOISTURE	MOISTURE	MOISTURE	MOISTURE	SOIL TYPE	6" T-180	MOISTURE	MOISTURE	MOISTURE	MOISTURE	MOISTURE
A-2-4 Spring Cem.	Test # 1	7.2	8.0	9.0	10.0	11.0	A-2-4 Spring Cem.	Test # 1	6.1	7.3	8.0	9.0	10.3
# 23462		DENSITY	DENSITY	DENSITY	DENSITY	DENSITY	# 23462		DENSITY	DENSITY	DENSITY	DENSITY	DENSITY
-200%: 14.8%		116.5	117.5	117.8	118.6	116.1	-200%: 14.8%		116.5	117.7	119.0	118.7	117.4
LL: NP		LBR	LBR	LBR	LBR	LBR	LL: NP		LBR	LBR	LBR	LBR	LBR
PI: NP		73	77	83	77	43	PI: NP		57	54	67	67	53
Mach.# 4							Mach.# 2						
Ht. 12.03"	Test # 2	MOISTURE	MOISTURE	MOISTURE	MOISTURE	MOISTURE	Ht. 18.00"	Test # 2	MOISTURE	MOISTURE	MOISTURE	MOISTURE	MOISTURE
wt. 5.51 lbs.		7.2	8.0	9.1	10.0	11.0	wt. 10.00 lbs.		6.1	7.4	8.1	9.1	10.9
Area: 2010.68mm		DENSITY	DENSITY	DENSITY	DENSITY	DENSITY	Area: 2000.75mm		DENSITY	DENSITY	DENSITY	DENSITY	DENSITY
		116.9	117.5	118.2	118.3	117.1			117.0	118.2	118.0	119.8	117.0
		LBR	LBR	LBR	LBR	LBR			LBR	LBR	LBR	LBR	LBR
		65	76	85	74	40			52	51	60	65	52
	Test # 3	MOISTURE	MOISTURE	MOISTURE	MOISTURE	MOISTURE		Test # 3	MOISTURE	MOISTURE	MOISTURE	MOISTURE	MOISTURE
		7.2	8.0	8.8	10.0	11.3			6.2	7.5	7.9	9.1	10.3
		DENSITY	DENSITY	DENSITY	DENSITY	DENSITY			DENSITY	DENSITY	DENSITY	DENSITY	DENSITY
		116.5	117.9	118.4	118.4	115.7			117.4	117.9	117.9	118.8	117.7
		LBR	LBR	LBR	LBR	LBR			LBR	LBR	LBR	LBR	LBR
		78	81	82	53	40			52	68	63	74	65
		MOISTURE	MOISTURE	MOISTURE	MOISTURE	MOISTURE			MOISTURE	MOISTURE	MOISTURE	MOISTURE	MOISTURE
	AVG.	7.2	8.0	9.0	10.0	11.1		AVG.	6.1	7.4	8.0	9.0	10.5
		DENSITY	DENSITY	DENSITY	DENSITY	DENSITY			DENSITY	DENSITY	DENSITY	DENSITY	DENSITY
	AVG.	116.6	117.6	118.1	118.4	116.3		AVG.	116.9	117.9	118.3	119.1	117.4
		LBR	LBR	LBR	LBR	LBR			LBR	LBR	LBR	LBR	LBR
	AVG.	72	78	83	68	41		AVG.	54	58	63	69	57

Table D-3. Branch Soil Densities for Single Sector Rammer

SOIL TYPE	4" T-99	MOISTURE	MOISTURE	MOISTURE	MOISTURE	MOISTURE	SOIL TYPE	4" T-180	MOISTURE	MOISTURE	MOISTURE	MOISTURE	MOISTURE
A-2-4 Branch	Test # 1	6.5	7.3	8.0	9.3	10.0	A-2-4 Branch	Test # 1	4.7	5.8	6.4	7.7	8.4
# 23477		DENSITY	DENSITY	DENSITY	DENSITY	DENSITY	# 23477		DENSITY	DENSITY	DENSITY	DENSITY	DENSITY
-200%: 21.8		123.4	125.3	126.7	126.5	125.5	-200%: 21.8		131.1	133.5	135.7	133.4	130.0
LL: NP							LL: NP						
PI: NP	Test # 2	MOISTURE	MOISTURE	MOISTURE	MOISTURE	MOISTURE	PI: NP	Test # 2	MOISTURE	MOISTURE	MOISTURE	MOISTURE	MOISTURE
Mach #5		7.0	7.8	8.5	9.5	10.3	Mach.# 1		4.5	5.5	6.7	7.8	8.9
Ht. 11.97"		DENSITY	DENSITY	DENSITY	DENSITY	DENSITY	Ht. 18.00"		DENSITY	DENSITY	DENSITY	DENSITY	DENSITY
Wt. 5.50lbs.		123.7	125.5	127.2	127.1	125.7	wt. 10.00 lbs.		129.8	132.6	134.1	133.2	129.3
Dia: 1.989"							Dia.: 1.997"						
	Test # 3	MOISTURE	MOISTURE	MOISTURE	MOISTURE	MOISTURE		Test # 3	MOISTURE	MOISTURE	MOISTURE	MOISTURE	MOISTURE
		6.7	7.8	8.5	9.5	10.2			4.7	5.7	6.7	7.4	8.5
		DENSITY	DENSITY	DENSITY	DENSITY	DENSITY			DENSITY	DENSITY	DENSITY	DENSITY	DENSITY
		124.0	125.2	126.9	126.6	125.2			130.2	132.7	134.3	133.7	130.3
		MOISTURE	MOISTURE	MOISTURE	MOISTURE	MOISTURE			MOISTURE	MOISTURE	MOISTURE	MOISTURE	MOISTURE
	AVG.	6.7	7.6	8.3	9.4	10.2		AVG.	4.6	5.7	6.6	7.6	8.6
		DENSITY	DENSITY	DENSITY	DENSITY	DENSITY			DENSITY	DENSITY	DENSITY	DENSITY	DENSITY
	AVG.	123.7	125.3	126.9	126.7	125.5		AVG.	130.4	132.9	134.7	133.4	129.9
SOIL TYPE	6" T-99	MOISTURE	MOISTURE	MOISTURE	MOISTURE	MOISTURE	SOIL TYPE	6" T-180	MOISTURE	MOISTURE	MOISTURE	MOISTURE	MOISTURE
A-2-4 Branch	Test # 1	6.4	7.6	8.5	9.4	10.4	A-2-4 Branch	Test # 1	4.3	5.3	6.5	7.4	8.2
# 23477		DENSITY	DENSITY	DENSITY	DENSITY	DENSITY	# 23477		DENSITY	DENSITY	DENSITY	DENSITY	DENSITY
-200%: 21.8		124.6	127.3	128.7	127.1	125.2	-200%: 21.8		129.3	132.1	134.5	134.1	132.1
LL: NP		LBR	LBR	LBR	LBR	LBR	LL: NP		LBR	LBR	LBR	LBR	LBR
PI: NP		40	57	39	18	7	PI: NP		73	102	160	111	56
Mach.# 4							Mach.# 2						
Ht. 12.03"	Test # 2	MOISTURE	MOISTURE	MOISTURE	MOISTURE	MOISTURE	Ht. 18.00"	Test # 2	MOISTURE	MOISTURE	MOISTURE	MOISTURE	MOISTURE
wt. 5.51 lbs.		6.3	7.6	8.5	9.3	10.4	wt. 10.00 lbs.		4.3	5.2	6.3	7.3	8.3
Area: 2010.68mm		DENSITY	DENSITY	DENSITY	DENSITY	DENSITY	Area: 2000.75mm		DENSITY	DENSITY	DENSITY	DENSITY	DENSITY
		125.5	127.9	128.4	127.6	125.7			128.9	132.1	134.0	134.2	131.3
		LBR	LBR	LBR	LBR	LBR			LBR	LBR	LBR	LBR	LBR
		35	53	43	19	4			69.0	124.0	165.0	118.0	55.0
	Test # 3	MOISTURE	MOISTURE	MOISTURE	MOISTURE	MOISTURE		Test # 3	MOISTURE	MOISTURE	MOISTURE	MOISTURE	MOISTURE
		6.4	7.7	8.5	9.4	10.4			4.2	5.3	6.5	7.5	8.3
		DENSITY	DENSITY	DENSITY	DENSITY	DENSITY			DENSITY	DENSITY	DENSITY	DENSITY	DENSITY
		124.6	127.6	128.0	127.6	124.6			128.8	132.0	134.7	134.1	131.5
		LBR	LBR	LBR	LBR	LBR			LBR	LBR	LBR	LBR	LBR
		40	49	42	22	8			75	132	147	120	48
		MOISTURE	MOISTURE	MOISTURE	MOISTURE	MOISTURE			MOISTURE	MOISTURE	MOISTURE	MOISTURE	MOISTURE
	AVG.	6.4	7.6	8.5	9.4	10.4		AVG.	4.3	5.3	6.4	7.4	8.2
		DENSITY	DENSITY	DENSITY	DENSITY	DENSITY			DENSITY	DENSITY	DENSITY	DENSITY	DENSITY
	AVG.	124.9	127.6	128.4	127.4	125.2		AVG.	129.0	132.1	134.4	134.1	131.6
		LBR	LBR	LBR	LBR	LBR			LBR	LBR	LBR	LBR	LBR
	AVG.	38	53	41	20	6		AVG.	72	119	157	116	53

D-4

Table D-4. Iron Bridge Soil Densities for Single Sector Rammer

SOIL TYPE	4" T-99	MOISTURE	MOISTURE	MOISTURE	MOISTURE	MOISTURE	SOIL TYPE	4" T-180	MOISTURE	MOISTURE	MOISTURE	MOISTURE	MOISTURE
A-2-4 Iron Bridge	Test # 1	7.0	8.1	9.0	10.0	10.9	A-2-4 Iron Bridge	Test # 1	7.0	7.6	8.3	9.1	10.1
# 23449		DENSITY	DENSITY	DENSITY	DENSITY	DENSITY	# 23449		DENSITY	DENSITY	DENSITY	DENSITY	DENSITY
-200%: 27.3%		117.2	120.7	123.0	123.6	122.0	-200%: 27.3%		126.4	131.3	132.0	128.7	125.6
LL: 21.6%							LL: 21.6%						
PI: 6.6%	Test # 2	MOISTURE	MOISTURE	MOISTURE	MOISTURE	MOISTURE	PI: 6.6%	Test # 2	MOISTURE	MOISTURE	MOISTURE	MOISTURE	MOISTURE
Mach #5		7.0	8.2	9.3	10.1	11.0	Mach.# 1		6.5	7.2	8.1	9.1	10.2
Ht. 11.97"		DENSITY	DENSITY	DENSITY	DENSITY	DENSITY	Ht. 18.00"		DENSITY	DENSITY	DENSITY	DENSITY	DENSITY
Wt. 5.50lbs.		116.9	120.1	122.4	123.2	122.2	wt. 10.00 lbs.		126.1	131.4	132.1	128.1	124.2
Dia: 1.989"							Dia.: 1.997"						
	Test # 3	MOISTURE	MOISTURE	MOISTURE	MOISTURE	MOISTURE		Test # 3	MOISTURE	MOISTURE	MOISTURE	MOISTURE	MOISTURE
		7.2	8.2	9.1	10.0	10.9			6.3	7.5	8.3	9.3	10.4
		DENSITY	DENSITY	DENSITY	DENSITY	DENSITY			DENSITY	DENSITY	DENSITY	DENSITY	DENSITY
		117.0	119.5	122.4	123.3	122.6			126.1	130.5	131.5	128.1	124.4
		MOISTURE	MOISTURE	MOISTURE	MOISTURE	MOISTURE			MOISTURE	MOISTURE	MOISTURE	MOISTURE	MOISTURE
	AVG.	7.1	8.2	9.1	10.0	10.9		AVG.	6.6	7.4	8.2	9.2	10.2
		DENSITY	DENSITY	DENSITY	DENSITY	DENSITY			DENSITY	DENSITY	DENSITY	DENSITY	DENSITY
	AVG.	117.0	120.1	122.6	123.4	122.3		AVG.	126.2	131.1	131.9	128.3	124.7
SOIL TYPE	6" T-99	MOISTURE	MOISTURE	MOISTURE	MOISTURE	MOISTURE	SOIL TYPE	6" T-180	MOISTURE	MOISTURE	MOISTURE	MOISTURE	MOISTURE
A-2-4 Iron Bridge	Test # 1	7.9	8.7	9.6	10.8	11.9	A-2-4 Iron Bridge	Test # 1	5.8	6.9	8.0	8.7	9.8
# 23449		DENSITY	DENSITY	DENSITY	DENSITY	DENSITY	# 23449		DENSITY	DENSITY	DENSITY	DENSITY	DENSITY
-200%: 27.3%		121.4	123.5	125.6	122.9	120.7	-200%: 27.3%		126.3	132.2	134.3	130.9	127.0
LL: 21.6%		LBR	LBR	LBR	LBR	LBR	LL: 21.6%		LBR	LBR	LBR	LBR	LBR
PI: 6.6%		18	22	17	5	2	PI: 6.6%		40	135	81	42	10
Mach.# 4							Mach.# 2						
Ht. 12.03"	Test # 2	MOISTURE	MOISTURE	MOISTURE	MOISTURE	MOISTURE	Ht. 18.00"	Test # 2	MOISTURE	MOISTURE	MOISTURE	MOISTURE	MOISTURE
wt. 5.51 lbs.		7.9	8.8	9.7	10.9	11.8	wt. 10.00 lbs.		6.1	7.2	8.0	9.0	10.0
Area: 2010.68mm		DENSITY	DENSITY	DENSITY	DENSITY	DENSITY	Area: 2000.75mm		DENSITY	DENSITY	DENSITY	DENSITY	DENSITY
		121.0	123.6	125.5	123.5	120.4			125.7	129.8	132.8	131.2	127.8
		LBR	LBR	LBR	LBR	LBR			LBR	LBR	LBR	LBR	LBR
		21	22	16	5	3			42	92	93	36	13
	Test # 3	MOISTURE	MOISTURE	MOISTURE	MOISTURE	MOISTURE		Test # 3	MOISTURE	MOISTURE	MOISTURE	MOISTURE	MOISTURE
		7.9	8.9	9.7	10.8	11.8			5.9	6.8	7.9	8.9	9.8
		DENSITY	DENSITY	DENSITY	DENSITY	DENSITY			DENSITY	DENSITY	DENSITY	DENSITY	DENSITY
		120.3	124.2	125.9	123.8	120.3			125.7	131.7	132.9	131.3	127.6
		LBR	LBR	LBR	LBR	LBR			LBR	LBR	LBR	LBR	LBR
		16	28	20	6	3			45	96	97	31	9
		MOISTURE	MOISTURE	MOISTURE	MOISTURE	MOISTURE			MOISTURE	MOISTURE	MOISTURE	MOISTURE	MOISTURE
	AVG.	7.9	8.8	9.7	10.8	11.8		AVG.	5.9	7.0	8.0	8.9	9.9
		DENSITY	DENSITY	DENSITY	DENSITY	DENSITY			DENSITY	DENSITY	DENSITY	DENSITY	DENSITY
	AVG.	120.9	123.8	125.7	123.4	120.5		AVG.	125.9	131.2	133.3	131.1	127.5
		LBR	LBR	LBR	LBR	LBR			LBR	LBR	LBR	LBR	LBR
	AVG.	18	24	18	5	3		AVG.	42	108	90	36	11

D-5

Table D-5. Summary of Densities from Double Sector Compaction Tests

DOUBLE SECTOR	MOISTURE	MOISTURE	MOISTURE	MOISTURE	MOISTURE	MOISTURE	MOISTURE
(A-2-4) Branch	6.8	6.9	6.8	6.7	6.8	AVG	6.8
MACHINE #2	DENSITY	DENSITY	DENSITY	DENSITY	DENSITY	DENSITY	DENSITY
	134.8	134.8	135.3	135.0	134.9	AVG	135.0
	1st PHASE	1st PHASE	2ed PHASE	2ed PHASE	2 PH. M #2	2 PH. M #2	2 PH. M #3
	4" T-180	6" T-180	4" T-180	4" T-180	6" T-180	6" T-180	6" T-180
MOIST.							
AVG.	6.6	6.5	6.1	7.6	6.1	7.6	5.9
DEN.							
AVG.	134.7	134.5	132.8	132.9	133.7	133.0	132.6
DOUBLE SECTOR	MOISTURE	MOISTURE	MOISTURE	MOISTURE	MOISTURE	MOISTURE	MOISTURE
(A-3) COAST ENG.	12.4	12.3	12.3	12.3	12.1	AVG	12.3
MACHINE #2	DENSITY	DENSITY	DENSITY	DENSITY	DENSITY	DENSITY	DENSITY
	111.1	111.5	111.3	111.3	111.5	AVG	111.3
	1st PHASE	1st PHASE					
	4" T-180	4" T-180	4" T-180	6" T-180	6" T-180	6" T-180	
MOISTURE							
AVERAGE	11.4	12.3	13.2	11.3	12.1	13.1	
DENSITY							
AVERAGE	111.1	110.4	109.2	109.8	110.6	109.4	
DOUBLE SECTOR	MOISTURE	MOISTURE	MOISTURE	MOISTURE	MOISTURE	MOISTURE	MOISTURE
(A-1-B) FL. ROCK	11.2	11.2	11.4	11.1	11.4	AVG	11.3
MACHINE #2	DENSITY	DENSITY	DENSITY	DENSITY	DENSITY	DENSITY	DENSITY
	110.4	110.4	110.7	110.7	110.3	AVG	110.5
	1st PHASE	1st PHASE					
	4" T-180	4" T-180	4" T-180	6" T-180	6" T-180	6" T-180	
MOISTURE							
AVERAGE	10.5	11.4	12.3	10.4	11.3	12.4	
DENSITY							
AVERAGE	109.8	110.0	109.2	108.0	108.9	108.7	